BUILDING AN ULTRAFAST CAMERA

4,6 trillion frames a second

Jeroen van den Brink
Bachelor Thesis
The Hague University - LENS institute Firenze

Date: 3rd of June , 2016.

Bachelor graduation thesis by:

Jeroen van den Brink
12051527

Internship mentor:
Prof. Dr. D. Wiersma wiersma@lens.unifi.it

Internship coach:
Dr. D.D. Land d.d.land@hhs.nl

2nd Assessor:
Ing. J.L. Van Yperen j.l.vanyperen@hhs.nl

Preface

In my graduation research I had the assignment to rebuild and upgrade a time-resolved setup. In my first two months I have built up and tested the setup as well as measured initial results. These results include time-resolved measurements with a photo multiplier tube and images of both paper and whispering gallery mode resonators.

As there was a power outage two months into my research the pump laser and optical parametric oscillator (Spectra-Physics OPAL) were not functioning anymore. As the parts to repair this came only in the last week of my stay in Italy, carrying out follow up measurements on the already found data was unfortunately impossible.

The upside of this was that I had a chance to further study the setup and the measurements that were taken, which provided some new insights in the setup as well as huge leap forward in the future of time-resolved measurements with this type of setup.

I also have been helping out PhD students in the research group, working in a clean room manufacturing tunable whispering gallery mode resonators and a light activated micro gripper, and I have been working on a model of the whispering gallery mode resonator in Comsol Multiphysics. These results will not be discussed in this thesis.

Acknowledgements

First I would like to thank Prof. Diederik Wiersma for giving me the opportunity to work at the LENS institute in Florence, Italy. Thanks to the whole Complex Photonics group and especially Sara Nocentini, Simone Zanotto, Francesco Utel, Amos Egel, Daniele Martella and Camilla Parmeggiani for keeping me company and having healthy discussions about work related subjects but mostly about Italy. A special thanks go to Lorenzo Pattelli and Dmitry Nuzhdin whom I worked with side by side in re-building this awesome setup which Lorenzo already made use of during his master studies, and Dmitry will continue to use during his doctorate studies.

Thanks to Ruben van der Sleen, for making the exquisite cover of this thesis and showing me that the Akzidenz-font is the way to go.

My parents, for their support through the past four years.

A final word of thanks goes to my girlfriend, Feike Fliervoet, who I lived in Italy with for four months. Thanks for all the times you wanted to hear me out about extremely boring stuff, the rereading of pages I wrote and helping me de-stress with some really nice trips to other cities nearby. Thank you.

Abstract

In this thesis the workings of a time-resolved setup are treated as well as the underlying physics. The setup is based on optical gating, which gives control over very short moments in time to let light pass through a gate. As this process is stable, light can be studied in very short and low intensities. When building this setup, first the "gate-open" time was measured (via cross convolution), the time the gate is open is 320 femtoseconds. When this is compared to a cross convolution measurement of the setup in 2012 it is now 90 fs longer open, which implies a degradation of the temporal resolution. The significance of this is low, as the measured samples have much longer decay times (20 ps).

After this an experiment was conducted of a light pulse (λ = 810 nm) travelling through a sheet of paper. The findings from this experiment are that there is some light going ballistically through the paper when the intensity peak in time is compared with and without the paper (the rising of the peak is both the same). Also from the decay of the intensity the transport mean free path is calculated, which describes the average length a photon is "walking" through the medium before it is scattering completely randomly. The transport mean free path is: 20±5 μm. Compared to earlier measurements, it is longer but still in the same degree of length. The cause of a longer transport mean free path can be that the paper used in earlier measurements was denser than the paper used in this thesis, resulting in more scattering events closer together. Also time-resolved images were made that shows the propagation of light through the paper in detail.

Finally, an experiment was conducted to see if a waveguide assembly with a whispering gallery mode resonator attached to it could be measured. In order to do so the setup needed to change, interchanging the probe and gate beam as the couplers of the waveguide are more susceptible to the wavelength of the gate beam. The Time-resolved change in intensity is measured from the output coupler as well as images from the pulse coming out of the coupler. This is a world's first in a wide field setup (as opposed to scanning pixel by pixel with a fiber). As the possibility for further research of the waveguide assembly was prohibited, the designation of the measured peaks is incomplete. Verification as well as more intricate waveguide assemblies belong to the future of this Time-resolved setup.

In appendix A, a brief note is given to the changing of the sum frequency generation crystal that is used in the setup. This crystal is the core of the optical gating technique, and changing the crystal from BBO to BiBO enhanced the spatial resolution almost tenfold. Because the setup was broken by a power outage, further research on this improvement was not an option, but a tentative insight is given into this positive outcome.

Contents

1. Introduction

Light moves at $3{,}0 \cdot 10^8$ $m \cdot s^{-1}$ [1]through vacuum but it slows down in the propagation direction when it encounters particles and light will interact with these particles; it reflects and refracts due to these particles. Light slows down more when the medium it goes through is denser as there are more particles. Eventually light will be absorbed or reflected completely.

In some materials light becomes scattered randomly in all directions. If a material scatters 100% of the light, the light is called diffusive. As this process is as fast as light travels, it is difficult to study this phenomenon in detail. For example, if light goes through paper, which is around 0,1 mm material (see chapter 4.4), it will take light 0,1 picosecond to go straight through this distance (the light speed in a medium is a fraction slower, this will be later explained). But because of scattering inside the structure there will be a percentage of light that will travel a longer distance through the paper and therefore takes a longer time to travel the distance of the paper.

The time-resolved setup described in this thesis can measure and image light transportation through diffusive materials (such as paper) by an optical gating technique. With this technique it is possible to choose for a very small time window which light can go to a measurement apparatus. This selection in time makes it possible to "freeze" the situation, therefore, as the laser is sending very short pulses inside the medium, the gating system makes it possible to measure the same time window for every pulse. The measurement and imaging system is limited in that it can only measure the surface of a medium.

In this graduation research an experimental time-resolved setup was rebuilt and later upgraded. This setup was used in 2012-2013 to conduct measurements by the "Optics of complex systems" research group of the LENS institute. These results are now published in the journal Light: Science & Applications as of May 6th (Nature publishing group)[2]. After the measurements were finished the setup was left derelict and was not working when the graduation research started.

This thesis will describe the theoretical foundations on which the workings of the time-resolved setup are based and the measurements conducted with this setup. It will first describe the measurements that have been conducted to analyze the temporal resolution of the setup. This outcome will be compared with the earlier measurements as a confirmation of the correct working of the setup.

Secondly, a time-resolved measurement of paper will be conducted to research the light diffusive properties of paper and to see the imaging sensitivity. As this measurement has been done before, it can also be used as a comparison. With the time-resolved intensity curve obtained from the measurements, it will be possible to calculate the transport mean free path. This length gives an indication to the average length a photon has to "walk" inside a structure before its scattering events are completely random.

Thirdly, the focus will shift to time-resolved study of light and light propagation in a photonic circuit with a whispering gallery mode resonator attached to it. This is the first time such measurements have been successfully conducted in a wide-field imaging setup (opposed to scanning pixel by pixel). After my graduation project has been completed, the research group will continue with this line of research.

Research questions:

- What is the temporal resolution of the rebuilt setup?

As a control to the quality of the setup, a cross convolution will be performed to measure the time the gate is open and light can go through. This will be compared to an earlier cross convolution measurement of the setup when it was running in 2012. Although the setup has changed between then and now, it will allow to see if the quality of the setup has degraded and give insight into the temporal resolution.

- What is the influence of paper on the length of an ultrafast pulse and how does light propagate through paper?

The setup is fast enough to measure the intensity of a pulse going through a piece of paper. Also imaging is possible of the light scattering through the paper medium. From the data the transport mean free path (l_t) can be calculated, this gives insight on how the light interacts with the paper.

- Is it possible to measure the Time-resolved transmission of the whispering gallery mode resonator and if yes, is it possible to image this?

As the efficiency of the in and output coupler is low, it is not known if the setup will be sensitive enough to measure and image the output light pulse of the whispering gallery mode assembly. When a signal can be measured by the photo multiplier tube it is possible to calculate the amount of times a pulse completes a roundtrip in the whispering gallery resonator.

2. Theory

In this chapter the different aspects of the Time-resolved setup are discussed and mathematical support is provided for this subject. Most of the literature used in these chapters is from the books: “Introduction to Optics”, “Optoelectronics and Photonics” and “Nonlinear Optics”. These are all later noted in the references.

Side note: The form of the mathematical expressions is based on the convention used by Boyd in his book “Nonlinear Optics”. This means that the negative (complex) frequency components are not taken into account; the difference between this and taking into account the negative frequency part of the complex notation is a factor of 0,5 for the *E* and *P* expressions in the chapters 2.2 and 2.3.

2.1 A short introduction into quantum mechanics

Light can be described as an energy package called a photon. The energy of this photon is completely dependent on its wavelength. The higher the wavelength the more energy this packet contains. This energy is depicted as electromagnetic radiation and can be calculated by the following formula:

$$E = h\nu \tag{2.1.1}$$

In which:

E	=	energy	[J]
h	=	Planck constant	[J·s]
ν	=	frequency	[s^{-1}]

The Planck constant is used as a quantification of light and matter. It is the smallest increment of energy an electrical oscillator can make in a hypothetical perfect cavity which absorbs all electromagnetic energy (a black body).

Because the energy of one photon is very low, most measurements measure a multitude of photons. These groups of photons are called wave packets, the energy of which can be calculated with the same expression as 2.1.1, but with the addition of a *n* integer.

$$E = nh\nu \tag{2.1.2}$$

n	=	number of photons	[-]

Even if there are no photons (complete darkness) there can be energy in the electromagnetic field. This ground state of the field means that the electromagnetic energy of a system can never be zero.[3] The theory behind this goes beyond the scope of this thesis, but an analogy is given to understand this zero-point energy, as this zero-point energy is later used to describe a certain photon-electron interaction.

Imagine that a room is filled with an enormous amount of fixed points which all have a weight with a spring attached to it (the oscillator). If there is no energy in this room, all weights will be exactly in the middle, where the spring will not push or pull at the weight.

In quantum mechanics there is an uncertainty principle (the Heisenberg uncertainty principle) which states that the precision of the position times the precision of momentum always has to be the same or larger than half of the Planck-constant. This in short, means that this uncertainty principle does not allow the weights not to be oscillating, there will always be a very small oscillation. When the integral of the whole room is taken, the energy will be exactly[3]:

$$E_{zp} = \frac{1}{2} h\nu \qquad (2.1.3)$$

The dependency of frequency in equation 2.1.3 is based on the assumption that the vibration of the oscillators are residuals of earlier electric waves passing through the system. As there is no system where there has never been any electric field, equation 2.1.3 is valid. To calculate the energy in a system the average frequency is used.

In stimulated absorption, atoms are surrounded by one or more particles carrying negative energy called electrons. These electrons orbit the core and are in different energy states[†]: when an electron gains distance from the core it gains potential energy, which is described as going to a higher energy state. These states are quantized; it is forbidden to reside in between states or to be in the same state as another electron (stated in the Pauli exclusion principle). When an electron is excited by, for instance, a photon with the energy that is similar to the difference between two states, the photon will transfer its energy to the electron. This in turn will make the electron jump out of its current orbit to a higher orbit around the core. An electron does not "want" to be in a high energy state. It will jump back to the lowest energy state possible (a lower state that is not already occupied by another electron) and in this process it must abide to the law of conservation of energy. As it has an excess of energy moving from a high state to a lower state, it will remove this excess of energy by releasing a photon. This is a very important process, because it is fundamental to making a material lase.

There are three types of photon-electron interactions: stimulated absorption (which is described above), spontaneous emission, and stimulated emission.

In spontaneous emission, an electron is in a higher energy state and "sees" an empty spot at a lower energy state. It will transfer to the lower state and emit a photon with energy $h\nu=E_2-E_1$. This type of emission cannot be controlled as there always will be electrons that are randomly excited to a higher state, for example by heat, impeded light or the fact that there is a ground state of the electric field which cannot be zero.

In stimulated emission (also known as induced emission) where an electron is at E_2 state and "sees" an incoming photon with energy equivalent to E_2-E_1 called a resonance photon[4], the electron will transfer to the lower energy state and will create a photon with exactly the same properties as the resonance photon. These properties include the direction, phase and polarization. In short, it is amplification of light. Stimulated emission is the principle through which a laser beam is

[†] *This is of course a very simplified view of the electron-core interaction and the energy states which an electron can reside, in reality there are no orbits but a probability field where an electron can reside. For the matter of this thesis it is enough to stay at this level of simplicity.*

generated, but for this process to happen there must be an excess of electrons in a high energy state. As described above, the electron prefers to reside in the lowest energy state, so a high energy state is not a place where an electron "wants" to be.
To make sure that stimulated emission is the main phenomenon occurring in the lasing material there should be more electrons in a higher energy state than in a lower energy state. This is called a population inversion: to have a constant population inversion the lasing material should be excited with energy to let the electrons stay in a higher energy state. In solid state lasers (like the ruby laser) this is mostly done by a flashtube. Nowadays, and also in the setup that is used in this thesis, this is done by a continuous pump laser beam which uses laser diodes. The diodes have a built-in population inversion because of the choice of used materials stacked in layers in a diode. These layers are doped with a material to create an excess of electrons or holes (respectively n or p junctions). When a current is applied over these layers, an electron will jump to the other layer and emit a photon.
A second prerequisite for a laser is to have an optical cavity made of two (or more) mirrors (this is a typical view of lasers, in principle "trapping" light is enough). One of these mirrors is a 100% reflecting surface, while the other is a surface close to 100% reflectivity (it will let some light through). The lasing material (also called gain medium) is in between the mirrors on the optical axis. When there is a population inversion in the lasing material there will first be photon generation by spontaneous emission (assumed that there are no stray photons in the optical cavity). These photons have random direction and phase distribution. If a photon is emitted not in the direction of the optical axis, it will leave the cavity, and will be extinguished. If the photon's direction is randomly coherent with the optical axis it will reflect back through the gain medium and there will be a chance that stimulated emission will occur. Subsequently, two photons will be reflected at one of the mirrors and returned to the gain medium, and the same process as described above will repeat, but now with two photons. This can also happen for photons that are relatively close to being coherent to the optical axis, although the amplification will be lower. As one of the mirrors is concave, the angle of the photon to the optical axis will increase for every return trip, meaning only the photon that arrives exactly in the middle will have no change in angle.
The time to complete one pass in the cavity is:

$$T = \frac{2L}{c} \tag{2.1.4}$$

In which:

T	=	time	[s]
L	=	cavity length	[m]
c	=	speed of light	[$m \cdot s^{-1}$]

When the amount of photons in the cavity is high enough, there will be losses because of the photons going through the second mirror and outside of the cavity (these are the photons that are useable for experiments). This loss, together with the amplification of coherent photons in the gain medium needs to find a balance: the amount of photons that pass through the second mirror cannot be higher than the amplification as this will cease the working of the laser. The time to complete one pass in the cavity is somewhat shorter because the cavity not vacuum. Light in a medium travels slower than the speed of light in vacuum, which is calculated by:

$$v_l = \frac{c}{n} \tag{2.1.5}$$

In which:

v_l = propagation speed of light [$m \cdot s^{-1}$]

n = refractive index of medium [-]

This concludes the normal start-up procedure of a (Fabry-Perot) continuous wave laser. The completion of this process a matter of microseconds. After this the laser will repeat the aforementioned process, which gives a continuous beam if the losses and gain are equal. This can be controlled automatically or by a passive system, debated in paragraph 2.4.

2.2 Linear optics[‡]

In the last paragraph light was seen as a (aggregation of) photon, a particle that moves and interacts with a mirror like a ball bounces off a wall. This is in fact partially true: light can exhibit particle behavior as well as wave behavior. Therefore, light is also characterized by wave equations. The simplest form of this equation is found below, which describes a travelling wave along the z-axis in vacuum[5]:

$$E(z,t) = E_0 e^{j(\omega t - kz)} \tag{2.2.1}$$

In which:

E	=	electric field	[N·C^{-1}]
ω	=	angular frequency	[rad·s^{-1}]
t	=	time	[s]
k	=	wave number	[m^{-1}]
z	=	distance	[m]

This equation describes that for an electric wave travelling in the z-direction in time, the amplitude will change by the angular frequency ω (the value of ω is calculated by: $2\pi\nu$, where ν represents the frequency in Hz) and the wave number k (which is also named propagation constant and is calculated by using: $k = 2\pi\lambda^{-1}$, where λ is the wavelength in m).

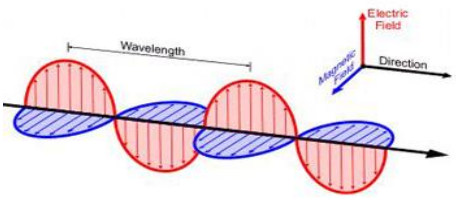

Figure 2.1, a schematic representation of a light wave[25].

The term wavelength (λ) is given by the distance the light wave has travelled for one oscillation of the electric field, as seen in figure 2.1.

According to the Maxwell-Faraday law, for an electric field that is changing in time there should be a magnetic field present perpendicular to the electric field and to the axis of propagation with the same angular frequency as the electric field. The dependence of the magnetic field and electric field is:

$$\frac{1}{2}\varepsilon_0\varepsilon_r E^2 = \frac{1}{2\mu_0} B_\perp^2 \tag{2.2.2}$$

In which:

ε_0	=	absolute permittivity	[C^2·m^{-2}·N^{-1}]
ε_r	=	relative permittivity	[-]
μ_0	=	magnetic permeability	[N·A^{-2}]
B	=	magnetic field	[A·m^{-1}]

[‡] *In this and the following paragraph, scalar approximations are used for the polarization and nonlinear behavior of dielectric materials.*

The absolute permittivity is the value of how the vacuum interacts with an electric field. In a way it is saying how much the vacuum permits the electric field to travel through itself. If an electric field is not travelling through a vacuum the permittivity is also not the same as in a vacuum, so a second constant is added called the relative permittivity. This relative permittivity is different for every material, calculated by:

$$n = \frac{c}{v} = \sqrt{\varepsilon_r} \tag{2.2.3}$$

In which:

v = phase velocity [$m \cdot s^{-1}$]

The phase velocity is the speed of the phase with which a wave is traveling, or observed differently: the speed of an antinode becoming a node or vice versa. The phase velocity in an isotropic medium is also calculated by:

$$v = \frac{1}{\sqrt{\varepsilon_0 \varepsilon_r \mu_0}} \tag{2.2.4}$$

The refractive index is a constant that gives an indication as to how much a reflected light beam is diverted from its original path when it hits a boundary of a medium with a different refractive index than the one the original light beam is travelling in (more information about refracting and scattering is in paragraph 2.6).

As lasers are normally not rated for the electric field they are generating but for the light intensity they are delivering, an equation is provided to calculate the intensity from an electric field to light intensity. First a pulse is described with an area of A and is moving with v in the z direction in a time Δt. The pulse has an energy flow (a change of the electric field) given by[5]:

$$S = \frac{(Av\Delta t)(\varepsilon_0 \varepsilon_r E^2)}{Av\Delta t} = v\varepsilon_0 \varepsilon_r E_x{}^2 = v^2 \varepsilon_0 \varepsilon_r E_x B_y \tag{2.2.5}$$

In which:

S = Poynting vector [$w \cdot m^{-2}$]
A = area of the pulse [m^2]

(the last two expressions in 2.2.5 are equal to $E_x = vB_y$[5])

The Poynting vector describes the total energy passing through the area A in a certain amount of time. The energy passing through this area is dependent on the phase velocity v.

As the wave is varying through time the average is taken of one period of the Poynting vector[6]:

$$I = S_{avg} = \frac{1}{2} v \varepsilon_0 \varepsilon_r E^2 \tag{2.2.6}$$

In which:

I	=	intensity	$[W \cdot m^{-2}]$

Using expression 2.2.3, expression 2.2.6 can be written as:

$$I = \frac{1}{2} cn \varepsilon_0 E^2 \tag{2.2.7}$$

On a side note, the correct term of the intensity stated here is the average irradiance. As there is a confusion between these two terms intensity is commonly used, but the correct name is irradiance.

Charged particles like electrons will respond to an electric field because of the negative charge they carry. In this paragraph the focus is on dipoles, molecules that have a positive core and electrons around it, with the unusual feature that it does not have a uniform distribution of electric charge[6]. When an electric field impinges on a medium, the electrons that are bound to the core of the atom will react and shift due to the electric field. They will start vibrating in accordance with the frequency of the light wave. Because of the shifting of the electrons, the atoms now become dipoles, particles which don't have an equal distribution of charge.

In classical physics the dipoles are seen as a positive charge particle (the core) and a negative particle (an electron) with a "spring" between them. The region (if the force applied to distance is plotted in a graph) where the distance between the two particles is equal to the amount of force applied to the dipole by the electric field is called the linear region. The interactions between dipoles and the electric field describe all the linear optics phenomena, such as refraction and polarization.

This is where classical physics and quantum physics overlap. If the negative and positive charged particles move away from each other, this can also be considered as an electron going to a higher energy state due to the extra energy it acquires from the electric field. Because the field is oscillating the field will also lower in intensity. The electron will lose this extra energy and move to a lower energy state (thus moving closer to the core).

The electric field displacement (or flux density) is the amount of energy going through a certain surface. This can be calculated by[7]:

$$D = \varepsilon_0 E + P \tag{2.2.8}$$

Where:

D	=	electric field displacement	$[C \cdot m^{-2}]$
P	=	Polarization density	$[C \cdot m^{-2}]$

There is a second variable needed to describe the electromagnetic field, which is the polarization of light. The polarization is the direction of the oscillation of the electric field. When an electric

wave encounters a dielectric material[§], the probability field (the field where an electron can reside) of an electron stretches in accordance to the polarity of the field (from a sphere to an oval). The polarization depicts this separation of charges as the electric field is going through a medium, in a sense they are the same, as they are dependent on each other (another way of seeing it that the electric field in a medium is called polarization). The dipoles in a crystal have a permanent structured orientation, which is also called polarization[**]. Both the polarization of a medium and the polarization of the electric field have to be the same for the electric field and the dipoles in the material to interact. When a light wave is travelling through a medium, due to the very high angular frequency of the electric field, the dipoles start vibrating with the same frequency as the light wave. When the material is not structured, there will not be a single polarization angle but all the dipoles will have a different angle, and the polarization of the light coming from the medium will be chaotic. Materials can be non-susceptible to certain polarization angles, for instance when the dipole polarization angle is 90 degrees from the electric field polarization.
The dependency of *E* and *P* in a medium is:

$$\tilde{P}(t) = \varepsilon_0 \chi^{(1)} \tilde{E}(t) \tag{2.2.9}$$

The tilde noted at P and E means that these values are oscillating rapidly in accordance to the oscillations of the electric field. The numbers in between () are indications of the order of generation (next chapter).

In which:

χ = electric susceptibility [-]

The susceptibility of a material is determined by the amount of change in polarization of a dielectric material in accordance with the impinging electric field. The higher its susceptibility, the "easier" it is for a material to react (polarize) according to said electric field. This in turn will make sure that the electric field will go freely through a material and will not build up energy inside it. These mediums are called linear. χ is related to the electric permittivity by[8]:

$$\chi^{(1)} = \varepsilon_r - 1 \tag{2.2.10}$$

This means that in vacuum (ε_r equals one) the susceptibility will be zero, which is imperative because there are no particles that can interact with the electric field. When expression 2.2.9 and 2.2.10 are known the electric field displacement can be written as:

$$D = \varepsilon_0 (1 + \chi^{(1)}) E = \varepsilon_0 \varepsilon_r E \tag{2.2.11}$$

this shows that the electric field displacement *D,* is the electric field that the material "permits" to be in the material. A note can be made that this will always be lower than vacuum.

[§] *A dielectric material is a material which doesn't conduct electricity (free electrons), but it's internal structure will respond to electric fields by charges that align themselves with the field polarity. A special case is the vacuum, where there are supposed to be no particles, but the creation of electron and positron pairs still allow an electric field to interact.*
[**] *When a medium has a non-chaotic internal structure it will have a polarization because the dipoles have their own electric field.*

2.3 Nonlinear Optics

Nonlinear response to an electric field gives opportunities to generate other wavelengths than light that is already travelling inside a medium. In this paragraph there will be a short introduction into the theory behind this.

In the last paragraph, the interaction from an electric field with a medium is ascribed to linear behavior, but in fact this is not true. For very high intensities the medium will respond in a nonlinear way to the electric field. This means that equation (2.2.9) is no longer valid as the polarization is no more linearly dependent on the electric field. As stated in the previous paragraph, the dipole is no longer in the linear region of the force-distance graph because the electron is saturated with energy. Equation 2.2.9 is expanded via taylor series development to:

$$\tilde{P} = \varepsilon_0 \chi^{(1)}(\omega)\tilde{E}(\omega) + \varepsilon_0 \chi^{(2)}(\omega)\tilde{E}^2(\omega) + \varepsilon_0 \chi^{(3)}(\omega)\tilde{E}^3(\omega) + .. \qquad (2.3.1)$$

In which:

$\chi^{(2)}$	=	second order susceptibility	$[m \cdot V^{-1}]$
$\chi^{(3)}$	=	third order susceptibility	$[m^2 \cdot V^{-2}]$

In Formula (2.3.1) there is also a second and third order susceptibility (the dependency on the inverse electric field will be addressed later in this chapter). The intensity of the electric field (and therefore the light wave) must be high to actually detect this phenomenon because of the low values of the electric susceptibility. Only certain crystals that do not have a high degree of structural order have a finite second order susceptibility[5]. The second and third part of the equation describe when the dipoles are no longer moving linearly in accordance with the applied force. More force is needed to move the dipoles the same amount of distance. When the input intensity is high enough, a second *P* will emerge: this polarization is generated by the dipoles itself, not the impinging electric field. This process can be written as:

$$\tilde{P} = \tilde{P}_L + \tilde{P}_{NL} \qquad (2.3.2)$$

Where the L and NL stand for linear and nonlinear.

When the expression 2.2.9 is used this means that there is a second electric field making up the total electric field generated by the medium. Therefore, equation 2.2.8 for *D* will expand, letting *D* be dependent on not only the linear *E* field but also on the *E* field that is generated by the polarization in the medium itself.

When the medium is dielectric and an electric field passes through, the negative charge from dipoles will rapidly start oscillating in accordance to the electric field. In a perfect situation the *E* field will oscillate sinusoidal; in the linear regime the *P* oscillations would also be the same. The dipoles will thus have the same oscillation frequency as the *E* field. In the non-linear regime, at very high intensities (an approximation of the needed intensity is given later), these oscillations will no longer be synchronized. The negative charges cannot keep up with the change of polarity.

Not all dipoles will behave like this, but a portion of the dipoles which are saturated with energy will start to act as its own electromagnetic emission source with a frequency of not one but two times the frequency ω of the incoming *E* field (see also paragraph 2.3.1). This makes it a second

harmonic generator. In short: These dipoles will actually start generating another light wave with a doubled frequency.

An approximation can be made for the value of the second and third order electric susceptibility, since the electrons in a dipole actually have to vibrate due to the electric field. The electric field that the light wave generates has to have the same order of magnitude as the electric field the electron creates (as the electron has a charge, it will create an electric field). This electric field is quite strong because of the small scale of the electron in comparison to its charge. First an expression for the electric field strength (E_{ef}) of an electron is stated[9]:

$$E_{ef} = \frac{e}{4 \cdot \pi \varepsilon_0 a_0^{\,2}} \tag{2.3.3}$$

In which:

e	=	electron charge	[C]
a_0	=	Bohr radius (hydrogen)	[m]

When a light pulse has an electric field with the same or higher power as the electric field strength of the electron the dipole becomes saturated with energy. When equation 2.3.3 is calculated, the electric field strength E_{ef} has a value of: $5{,}14 \cdot 10^{11}\ \mathrm{V \cdot m^{-1}}$. For vacuum the first order susceptibility will be equal to one. The second order and first order are related by the following expression:

$$\chi^{(2)} = \frac{\chi^{(1)}}{E_{ef}} \tag{2.3.4}$$

This approximation has a result of: $1{,}94 \cdot 10^{-12}\ \mathrm{m \cdot V^{-1}}$, which is accurate when compared to measured values[10] (it is in the same order of magnitude). The third order susceptibility has the same dependence on the first order susceptibility but E_{ef} is squared in equation 2.3.4.

Above stated approximations are made by using the simplest atom available to us, the hydrogen atom. When the atoms become more complex, the electric field strength of multiple electrons has to be calculated which is complicated, because of the different distances of the electrons to the core.

To excite a crystal to the point of electron saturation, which is when a nonlinear effect will happen, a tremendous amount of energy has to be focused on a material. As the electric field of an electron is known an estimation can be made of needed intensity by using expression 2.2.7:

$$I = \frac{1}{2} \cdot 8{,}85 \cdot 10^{-12} \cdot 3 \cdot 10^{8} \cdot \left(5{,}14 \cdot 10^{11}\right)^2 = 3{,}5 \cdot 10^{20}\ \mathrm{W \cdot m^{-2}} \tag{2.3.5}$$

This is a very high intensity, and only pulsed lasers will be able to make such an electric field.

The energy of the electric field coming out of a second harmonic generation can be approximated by using expression 2.2.1, only taking into account the second order of the expression:

$$\tilde{E}_{2\omega}(t) = \sqrt{\frac{\tilde{P}_{NL}^{(2)}(t)}{\varepsilon_0 \chi^{(2)}}} \tag{2.3.6}$$

it is stated in formula (2.3.6) that the energy of the electric field will be in accordance with the polarization field of the second harmonic. This is of course an approximation, only valid when the medium where the second harmonic frequency generation is taking place is homogeneous, lossless, and scatter free.

As the efficiencies of second harmonic generation are not 100%, the second harmonic will be travelling inside the medium while the beam that is driving this process (which lost intensity) is also travelling in the same optical path. Extraction of the second harmonic is done by using filters or introducing a prism[11].

A large impact on the efficiency of this process is that the individual phases of the incoming beam and the generated second harmonic beam are matched. This means that all the contributions from the molecules in the propagation direction are in the same phase or in a relation to each other at the exiting end of the medium. This is described in the momentum conservation law[12††]:

$$\frac{n_{\omega 1}}{\lambda_1} = \frac{n_{\omega 2}}{\lambda_2} \tag{2.3.7}$$

This means that the phase of the different wavelengths has to be in phase or the efficiency of the process will be so low that no second harmonic can be obtained.

The medium that is used should exhibit specific refractive index per wavelength. This narrows down the choice of material for something that is anisotropic (a material which does not have the same refractive index for every direction - polarization).

An Δk of zero is almost impossible. To approximate this as close as possible to this there are various solutions: Changing the angle of incidence, changing the polarization of the incoming beam or the technique of birefringent phase matching. The Latter works only when the crystal is birefringent (the refractive index is dependent on the polarization and angle of propagation). For the incoming beam and generated beam there are different refractive indexes, but they both depend on the temperature of the crystal itself. There is a temperature where both wavelengths have the same refractive index, resulting in a phase matching condition.

†† The expression is derived from the expression $k_1 = k_2$. As propagation number is conserved and is also calculated by $k=n\cdot\lambda^{-1}$.

2.3.1 Nonlinear optics applied to this setup

It is possible to create a different output light when two different light beams enter a nonlinear medium. This special phenomenon in nonlinear optics is the sum frequency generation (SFG). For this to happen the frequencies of the two light pulses that are impinging on the crystal do not have to be the same. There are however, some limitations to the choice of frequency. Since the phase matching condition still applies.

Other prerequisites must be met before this phenomenon will occur. First of all, the incoming pulses must have very well defined polarizations (linear polarization with a minimum of stray polarization for the BiBO crystal)[13]. Also the SFG crystal described in this thesis is not heated so the angle of incidence of the two beams and the overlapping of the beams must be very precise for maximum efficiency.

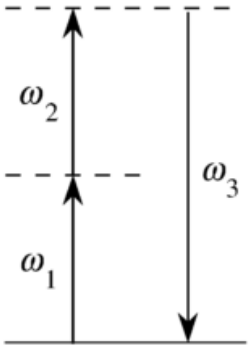

Figure 2.2, an example of the energy diagram for sum frequency generation, adapted from[9].

The mathematical expression for the electric field this phenomenon creates is:

$$\tilde{P}(\omega_1+\omega_2)=2\cdot\varepsilon_0\varepsilon_r\chi^{(2)}\tilde{E}_1\tilde{E}_2 \tag{2.3.8}$$

It is stated that the polarization in the medium is dependent on both the electric fields that are being inputted. This process is not optimal, so the output from the material will have three different wavelengths.

Quantum mechanically speaking both photons excite the electron to virtual states, which is a state so short lived that it is not observable. However, it is necessary to explain the energy difference from the two input beams to the output beam, as the state in the middle is not a quantized state for this molecule. The interaction is drawn schematically in figure 2.2.

The momentum conservation of this process is described by:

$$\frac{n_{\omega p}}{\lambda_p}+\frac{n_{\omega g}}{\lambda_g}=\frac{n_{\omega s}}{\lambda_s} \tag{2.3.9}$$

In which p denotes probe, g denotes gate and s denotes the signal beam.

From now on, this phenomenon will be called up conversion. This is because of the shorter wavelength that is coming out of the crystal than the two wavelengths that come into the crystal.

Another phenomenon used in this setup is the difference frequency generation (DFG, also called down conversion) in the optical parametric oscillator (OPO) and it can be seen as the direct inverse of sum frequency generation. The energy diagram follows the same energy levels (in reverse), but this time the state is not virtual. The input wavelength is split into two different wavelengths through the use of a birefringent crystal which exhibits this DFG phenomena (LBO – Lithium Triborate). The process is described mathematically as follows:

$$\frac{n_{\omega pu}}{\lambda_{pu}}=\frac{n_{\omega g}}{\lambda_g}+\frac{n_{\omega i}}{\lambda_i} \tag{2.3.10}$$

In which pu denotes pump, g denotes gate and I denote the idler beam.

As the conversion efficiency is much lower than the efficiency of the SFG process the input beam is oscillated through the crystal. To keep the same femtosecond pulse width the oscillation cavity of the OPO must be of the same dimensions as the Ti:Sa laser. This is actively controlled by the control system of the OPO to match the cavity length of the laser.

2.4 Mode locking Oscillator

The experimental setup treated in this thesis needs very short pulses, near 100 femtoseconds. To acquire these extremely short pulses an active mode locked Titanium sapphire laser is used (Tsunami, Spectra-Physics). This laser needs to be pumped by a continuous laser source (Millennia Xs, Spectra-Physics).

As the Titanium sapphire rod inside the Tsunami is pumped by the diode pump laser, the rod will start lasing. In the optical cavity of the laser there are two end mirrors (one of which is the output mirror and thus is not completely reflective). The distance between these two mirrors is the optical cavity length (L). In the cavity many standing waves of light can be present, as long as the wave "fits" inside the cavity (this means the wave constructively interferes with itself every roundtrip). These standing waves are called modes, and the amount of modes permitted in a cavity is calculated by:

$$q = \frac{2L}{\lambda} \tag{2.4.1}$$

In which q is an integer denoting the number of modes allowed in the cavity.

A quartz crystal is located just before the output mirror. This quartz crystal is an acoustic-optic modulator (AOM); on this crystal a piezoelectric transducer is added on the one end, and an absorber on the other end. The transducer lets the crystal vibrate with a certain frequency which ensues a standing wave in the crystal, creating a time dependent refractive index change inside the crystal. This is because when the soundwave is travelling through the crystal there is a certain strain build up inside the crystal. The strain from these vibrations on the crystal lets it contract or expand thus changing the density of the crystal. When the density is changed, the refractive index will also change as this is dependent on the density[‡‡]. This phenomenon is called the photo elastic effect. The dependency of refractive index on strain is[5]:

$$\Delta \frac{1}{n^2} = pS \tag{2.4.2}$$

In which:

p	=	photoeleastic coefficient	[-]
S	=	strain	[-]

Both p and S have no dimension. These numbers are properties of a material and are experimentally obtained.

To get the laser in a mode locked state, the piezo element lets the crystal vibrate at a frequency which is the same frequency as the repetition rate (the amount of pulses per second). By doing this the crystal is periodically creating a loss inside the cavity, which is similar to adding a shutter inside the cavity. Only light that is bouncing in between the two mirrors and arriving at the AOM at exactly the right time is let through by the crystal and is amplified in the gain medium. The rest

‡‡ Actually, due to the strain the bonds between the molecules are slightly distorted. This also changes the field in which an electron can reside in.

of the light is dumped outside of the cavity due to the losses created by the AOM (these losses are made by a different refractive angle at the output side, in which the light will not have an optimum path inside the cavity and will thus extinguish). The amount of loss is around 1%. This is enough to let the output become pulsed, as the modes that are let through by the AOM have a much higher gain due to repeated passes through the lasing material. Also the lasing material exhibits more gain when the intensity through the material is higher. An example of intensity in time can be seen in figure 2.3.

The laser used in this thesis uses a technique called regenerative mode locking, which does not change the length *L*, but only the frequency of the AOM. Because of this, there is a small feedback circuit with a photo diode looking for an initial "beating" of the fundamental modes (the primary and second harmonic). As the cavity length *L* is fixed in the Tsunami, the AOM needs to adapt its frequency to the time it takes for a light wave to travel through the cavity (the time is dependent on the temperature, humidity etc).

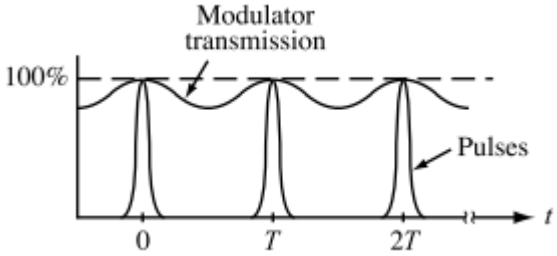

Figure 2.3, a standard active mode locking laser explained. Y-axis is intensity of the pulse and the transmission (loss) of the modulator. The X-axis is time. T stands for a round trip in the cavity. Adapted from[1].

The width of one Gaussian pulse at full width half maximum (FWHM) is determined by[1]:

$$\Delta t = 2\sqrt{\frac{\ln 2}{2\Gamma}} \tag{2.4.3}$$

In which:

Δt	=	pulse width FWHM	[s]
Γ	=	pulse width parameter	[s^{-1}]

To ensure the shortest possible pulse width, the parameter Γ must be as big as possible, which is calculated by:

$$\Gamma = \frac{1}{4\sqrt{2}} \cdot \sqrt{\frac{\Delta_m}{g}} \cdot f_m \cdot f_g \tag{2.4.4}$$

In which:

Δ_m	=	modulation depth	[-]
g	=	gain factor	[-]
f_m	=	repetition rate	[s^{-1}]
f_g	=	peak optical gain frequency	[s^{-1}]

The modulation depth is an index of how much the AOM has to change from its carrier signal to still ensure mode locking ($\Delta f/f_m$). This means that when the frequency of the AOM is set to the repetition rate that is required, there are slight changes in frequency depending on air quality and vibrations inside the laser assembly. The gain factor is the amount of energy added to the pulse in the gain medium, and the saturation (maximum) of this gain must be slightly higher as the losses transduced by the AOM, otherwise the cavity will be deprived of energy in a few roundtrips. As the lasing material adds energy to a broad spectrum of frequencies around a central peak travelling through it while travelling through it. This peak is called peak optical gain frequency.

2.5 Optical Gating

In this thesis, measurements and images are made by using a method called optical gating. By using this, it is possible to choose the moment of measurement very precisely. For example, if there is a light pulse generated by the laser (Tsunami 810 nm, 100 femtoseconds wide[12]), and inserted into a second oscillator (Opal), then the oscillator will create three different pulses. One of these pulses will stay the same wavelength (probe beam) This is the beam that will interact with the sample. The second is up converted to a higher infra-red wavelength (1550 nm). This beam is called the gate beam, and it will not interact with any material except the mirrors and the air it travels through. The third is the idler output which has a wavelength of 1700nm. The idler beam will not be used in this experiment. A side note is that the naming of these beams are arbitrary, as later shown in this thesis when they are interchanged.

When the probe beam is incident on a sample, the velocity will not be *c* (actually the light will still be very close to *c* but because the light will scatter inside the medium, it will travel a longer distance when only taking into account the z-axis) and the probe beam will take longer to travel the same path than without a sample due to scattering inside the sample. Because the probe beam has encountered a sample, it will be slower to arrive at the crystal. But in its intensity distribution there will be a trace of how this beam interacted with the sample.

If the gate beam's path can be controlled in the positive direction (this means that the beam path will be longer) the two beams can be synchronized again. When these two beams impinge on the SFG crystal it will create a third light wave with a frequency that is the sum of the two incoming wavelengths as is described in paragraph 2.3.1. As one of the two pulses is much shorter than the other, specific time windows of the process can be studied.

The intensity going through the gated system can be described as the convolution[§§] of the two pulses that are arriving at the SFG crystal[***12]:

$$I_s(\Delta\tau) \propto \int_0^\infty I_p(\mathrm{t}) \cdot I_g(t-\Delta\tau)dt \qquad (2.5.1)$$

s stands for signal, p for probe and g for gate pulse

In which $\Delta\tau$ represents the time difference between the probe and gate beam. An approximation can be made to further simplify this equation: when the gate pulse is denoted as a zero point in time. This assumption is reasonable when it is compared to the large time difference in pulse width between the probe and gate pulse (the probe pulse is several orders of magnitude longer in time than the gate pulse). This is depicted in figure 2.4.

[§§] *The integral of the surface in which both pulse intensity profiles overlap.*
[***] *Not taking into account the losses taken from the SFG process.*

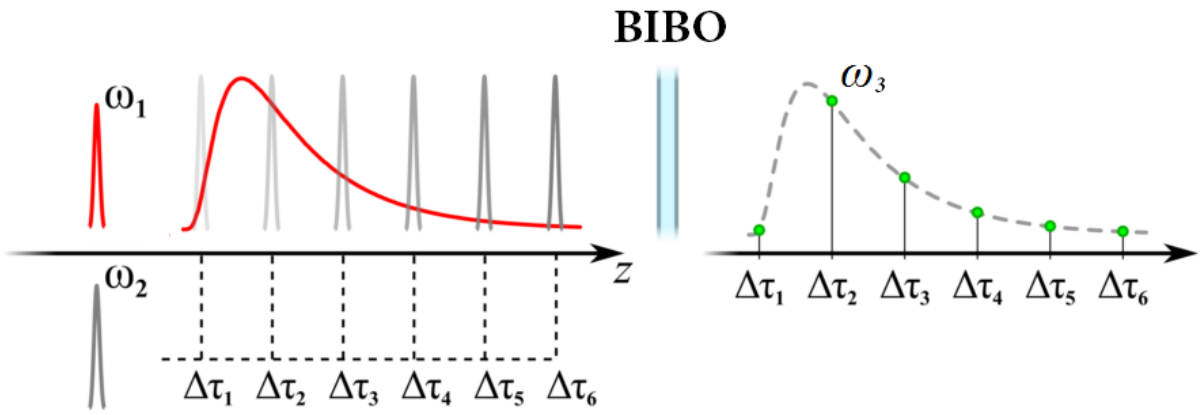

Figure 2.4, an example of the intensity-time distributions of the two input beams where the red (ω_1) is the probe pulse, the grey(ω_2) is the gate pulse and the green (ω_3) is the up converted signal pulse (adapted from[12]).

When equation 2.5.1 is changed by approximating the probe pulse as a Dirac function the equation can be written as:

$$I_s(\Delta\tau) \propto I_p(0) \cdot I_g(\Delta\tau) \qquad (2.5.2)$$

This simplification of equation 2.5.1 states that the intensity of the signal beam (not taking into account the low efficiency that occurs due to the sum frequency generation process in the crystal) is dependent on the intensity of the probe beam times the intensity of the gate beam at a certain delay. This delay moment ($\Delta\tau$) can be chosen due to the use of a moveable stage (translation stage). In figure 2.4 this procedure can be made visible by shifting the grey intensity peaks left and right, while the red curve stays at the same position. As stated before it is actually not the gate beam that is being delayed but the probe beam. This interchangeability between which beam is delayed is allowed because it is only the relative delay that matters in the above integral. Therefore, it does not matter if the probe beam or gate beam is delayed: as the output from the gate system is the same. It is said that the gate beam is delayed purely for logical convention.

The choice to delay the probe beam is made because of practical reasons: the probe beam is in the visible range and therefore easier to aim (as the precision of the alignment of the probe beam due to the moving of the two mirrors on the translation stage is critical).

After the three different wavelengths exit the crystal, the new pulse called the up converted or signal beam is easily extracted with the use of a bandpass filter and redirected to a Photo Multiplier Tube. To image an extra set of optics is used after the crystal to focus the image on the CCD-camera.

2.6 Scattering

In this paragraph a small introduction is given to what scattering actually is. First the interaction of a light beam is described when it is reflected from a different medium than it is travelling in. After this, the theory behind scattering from a medium and inside a medium is explained. The theory that is treated in this paragraph is loosely based on the PhD thesis of Dr. L. Cortese: "Light transport in complex photonics structures" and the book "Introduction to optics" by Pedrotti et al.

To make things simple light is first approximated as a ray (a line that is neglecting all wave properties of light), This particular part of optics is called geometrical optics. In this branch of physics, it is simple to describe how light interacts with a boundary between two different media, when light is already travelling in one of those media. There are two possibilities, either the ray is reflected with the same angle as the incoming beam has (according to the boundary), for the ray is not reflected at a boundary between two media but there is (a part) going through the second medium, the latter ray is called the refracted ray. This is described by Snell's law:

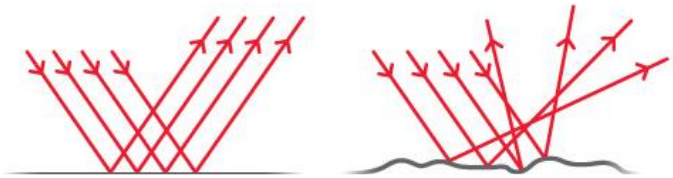

Figure 2.5, left a mirror like reflection, on the right a reflection from an irregular surface (Adapted from[26]).

$$n_1 \sin(\theta_I) = n_2 \sin(\theta_t) \tag{2.6.1}$$

The left hand side of the equation is describing the input ray travelling in a certain medium which has a refractive index of n_1. The right part describes the ray that is refracted from the boundary into the second medium with an angle θ_r. This law is only applicable when a light ray hits a boundary between two media with different refractive indices (if the medium has the same refractive indices, the beam will not refract as there is no boundary). Also when the input light ray is perpendicular to the axis of the medium the refracted light will go straight.

The amount of light that is reflected can be calculated by:

$$R = \frac{\frac{n_2}{\cos(\theta_t)} - 1}{\frac{n_1}{\cos(\theta_i)}} \Big/ \frac{\frac{n_2}{\cos(\theta_t)} + 1}{\frac{n_1}{\cos(\theta_i)}} \tag{2.6.2}$$

Where R stands for the reflectivity, the denotion of I and t are used for incidence and transmitted beam.

the transmission of a ray is dependent on R by a factor of $T = 1 - R$.

When light is not seen as a single ray and the encountered boundary not perfectly flat (like a mirror), the light is not reflected in one direction only, but the light is reflected to every angle randomly. This is depicted on the right side in figure 2.5.

This can happen at the surface of a boundary, but as mediums do not have an equally distributed density light can refract(enter) the medium. After this it can encounter a denser segment of the medium where it can reflect (as the refractive index is dependent on density). And keeps reflecting below the surface of the medium. In this thesis paper is examined. As can be seen from pictures

3.3 in paragraph 3.1 taken with a surface electron microscope (SEM), paper is not flat at all. And it is easy to see that light can travel through the medium because of the huge spacing between the paper fibers. The medium in between the paper fibers is air, which has a different refractive index with respect to the paper itself. When taking into account not one ray, but trillions of rays at the same time, the intensity of light at a certain point is the addition of all the scattering events happening at that moment. There is need for a statistical analysis to describe this process. Time-resolved measurements are one of these statistical analysis, as measuring one time-window is actually the average of multiple scattering occasions. A different approach is to simulate this by using Monte Carlo simulation. Although the results are in accordance with measurements, the calculation time is extremely long[12].

As the light that comes out of a medium which scatters is widened in the temporal domain it is concluded that light travels longer in a medium than in air. To compute the average distance a photon travels in a medium a few new concepts must be introduced. First, the average scatterings free path inside the material has to be derived. This is done by[12]:

$$l_s = \frac{1}{\rho \sigma_s} \tag{2.6.3}$$

In which:

L_s	=	average scattering free path	[m]
ρ	=	density of scatterers	[m^{-3}]
σ_s	=	scattering cross section	[m^2]

The scattering cross section stated in formula 2.6.3 is describe as the effective area interacting with a light particle. As the scattering event that is described in this thesis is anisotropic[†††] the properties of transmittance through a medium depend on the average distance a photon 'walks' before it completely "forgets" its incoming direction (g is zero). This may take several (anisotropic) scattering events before the photon is isotropically scattered[12]. This distance is called the transport mean free path:

$$l_t = \frac{l_s}{1 - g} \tag{2.6.4}$$

In which:

l_t	=	transport mean free path	[m]
g	=	anisotropy factor	[-]

The anisotropy factor of a scattering event is calculated by measuring the scattering probability distribution at different angles in the horizontal and azimuthal plane. The factor is a number from 0 to 1. If g is zero, the scattering is isotropic (randomly in every direction). If g is close to one the scattering event is still random but forward direction is more likely.

[†††] *If a scattering event has a high amount of intensity going into the same direction as before the event, it is called anisotropic.*

It can be concluded from this that when a light pulse hits a diffusive medium, the light will propagate through many different random paths through the material, eventually resulting in a bell shaped profile outward in the medium from the point of entrance.

The scattering free path will be shorter than the transport free path (it can also be the other way around, when g is < 0, but this is not the case with paper).

To calculate the transport mean free path an expression is used to calculate the transmission through a finite slab of scattering structure, this means using diffusive theory of light[14]:

$$sI = D_0 \frac{\partial^2 I}{\partial z^2} + \delta(z - l_s) \tag{2.6.5}$$

In which:

D_o	=	diffusion coefficient	[$m^2 \cdot s^{-1}$]
s	=	laplacian conjugate of time	[-]
z	=	distance through slab	[m]

D_0 can be calculated by taking the speed of light inside the material times the average step length. The expression 2.6.5 is in laplacian. When the expression is solved for the transmission and converted back in normal time the expression will be:

$$T(t) = \frac{2D_0\pi}{L_e^2} \sum_{n=1}^{\infty} \left(n(-1)^{n+1} \sin\frac{n\pi(l_s + z_e)}{L_e} \cos\frac{n\pi z_e}{L_e} \right) e^{\frac{-n^2\pi^2 D_0}{L_e^2} t} = Ae^{-\frac{t}{\tau}} \tag{2.6.6}$$

(A more extensive overview of transforming these equations can be found in the PhD thesis of Pierre Barthelemy[14], page 16 - 20).

In which:

z_e	=	(fictional) extrapolation length	[m]

the extrapolation length is acquired because of a flaw in the diffusion theory. The theory cannot handle finite media, this is why there is an extrapolation length, a point in space where the intensity will always be zero. This is because there are no boundaries from a medium to air for example. For this reason, also outside exposure (a light beam coming into a material from another medium) is not possible. The light is actually modelled as coming from inside the material, a little bit after the normal insertion point of light. to overcome this problem. When the intensity is plotted on the z-axis and this curve is extrapolated outside of the medium, there is a position on both sides of the medium where it hits zero. This position is called the extrapolation length. This length can be calculated by the following expression[14]:

$$z_e = \frac{2}{3} l_t \cdot A(n) \tag{2.6.7}$$

In which:

$A(n)$	=	function	[-]

This function *A* is a coefficient that depends on the refractive index mismatch of the boundary of two different media. To calculate this coefficient a very long expression is used which keeps

expanding. But as Contini et al. stated in his paper[15]: "*The equation for A is complicated. To obtain simpler expressions for practical applications, a polynomial fit was performed*.". This fit is also used in this thesis and can be found in paragraph 5.2.

To understand equation 2.6.6, the first part before the summation gives a reduction in intensity, as the intensity cannot be the same as the intensity before the scattering event. The second takes every scattering event and gives it a direction and a gradation of decay of intensity. This equation gives the mathematical expression for the later measured time-resolved signal through paper.

As the measurements in this thesis can only measure one decay (τ) variable (the slowest, which can be extrapolated from the decrease in intensity trend line after the initial ballistic impact of a pulse into the material) it is assumed that *n* equals 1 and *t* goes to infinity. As the focus is on discovering the τ and the transport mean free path (l_t) in this thesis.

Expression 2.6.6 is simplified by considering late times. At late times only the slowest exponentially decay contribution will dominate, which allows to consider only n=1.

$$\tau = \frac{{L_e}^2}{\pi^2 D_0} \tag{2.6.8}$$

In which:

τ = decay coefficient [s^{-1}]

Using the relations[14]:

$$D_0 = \frac{v \cdot l_t}{3} \tag{2.6.9}$$

$$L_e = L + 2z_e \tag{2.6.10}$$

In which:

L = Slab length [m]

Using the expression above, expression 2.6.8 can be rewritten as:

$$\tau = \frac{(L+\frac{4}{3}\cdot A(n)\cdot l_t)^2}{\frac{1}{3} l_t \cdot v \cdot \pi^2} \tag{2.6.11}$$

As the only unknown in this hyperbolic function is the transport mean free path, the only two unknowns are the τ and l_t. When the τ is extrapolated from the paper measurements, the l_t can be calculated by solving the equation. This solving will be done by an external solving program, written by the author in Matlab. More details about this program can be found in appendix D.

2.7 Waveguides

To let light travel inside a structure without refracting from it, the structure needs to have a refractive index higher than its surroundings. As a convention the inner structure (where the light travels) is called the core with a refractive index denoted as n_1 and the outer layers is called the cladding with a refractive index denoted n_2. Light can propagate through the core with a zigzagging motion, bouncing from its core-cladding boundaries. Even when the core is bent and the direction of the material is not straight this behavior will continue. This is called a total internal reflection (TIR), meaning that every reflection it makes it is constructively interfering with itself through the structure, and when this happens the structure is called a waveguide. For a waveguide to support this total internal reflection it has to satisfy the following condition[5]:

$$\frac{2\pi n_1 d}{\lambda} \cdot \cos(\theta_m - \phi_m) = m\pi \tag{2.7.1}$$

In which:

d	=	thickness	[m]
θ_m	=	angle of incidence	[rad]
φ_m	=	relative phase	[rad]
m	=	mode number	[int]

The denotation of the subscript m with the angle of incidence and phase is because these two are dependent on the integer value of m. Only one angle and one phase condition are allowed to have total internal reflection for every mode there is.

To inject a light pulse inside a waveguide, the light pulse must have an angle greater than the critical angle θ_c. The critical angle can be calculated by:

$$\theta_c = \sin^{-1}\left(\frac{n_2}{n_1}\right) \tag{2.7.2}$$

Also for TIR the angle of incidence (θ_m) has to be greater than θ_c.

An electric field travels through a waveguide via different modes. Meaning: a light ray that is travelling through the waveguide with a particular angle in respect to the cladding-core boundary. with each different arrangements of intensity. These modes can be electric or magnetic[‡‡‡], the first is the TE (electric) mode, this means that the electric field is moving through the walls of the waveguide and are perpendicular to the to the propagation direction. With the other mode called TM (magnetic), the electric field is now moving inside the waveguide and the magnetic field is oscillating through the waveguide perpendicular to the propagation direction.

The intensities of these fields are quantified and noted in a subscript with two integers. A single mode fiber will have one dominant mode of propagation, this will be denoted as 00 and will have a Gaussian intensity curve with its maximum in the middle of the waveguide. The first integer gives the amount of maxima in intensity in the horizontal plane, while the second integer is the

[‡‡‡] *In real-life situation there is a not a pure TE or TM field. There will be a mix of the both called a TEM mode. As the polarization will not be completely linear.*

denotation for the amount of maxima in intensity in the vertical plane. This is also seen in figure 2.6.
A 10 mode will have two maxima in intensity when it is observed from left to right in the middle of the pulse, and so on. The maxima will be at position of $\lambda/2$ times the number.

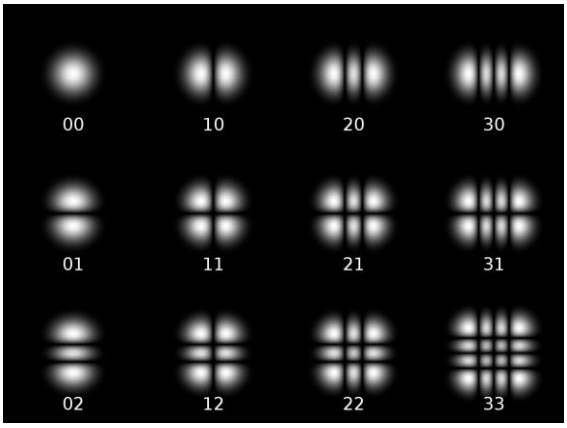

Figure 2.6, a visual representation of different field intensities in a square waveguide (adapted from[27])

There is also a buildup of the electric field inside the cladding. This penetration into the cladding is called the evanescent wave. The higher the mode of the light travelling through a waveguide, the more intensity "leaks" into the cladding. This leaking can be measured[16] or used to inject light into a structure that is not directly connected to the waveguide itself (as is done in this thesis).
The amount of penetration inside the cladding is calculated by:

$$\delta = \frac{\lambda}{2\pi n_2 \sqrt{\left(\frac{n_1}{n_2}\right)^2 \left(\sin^2(\theta_m) - 1\right)}} \tag{2.7.3}$$

In which:

δ	=	penetration depth	[m]

This is the depth where 63% of the energy is absorbed into the material[5]. The intensity at a certain point is calculated by using the law of Lambert-Beer:

$$\mathrm{I}(x) = \mathrm{I}_0 \, e^{-\alpha x} \tag{2.7.4}$$

In which:

α	=	absorption coefficient	[m^{-1}]
I_0	=	Intensity at the boundary	[$W \cdot m^{-2}$]

The absorption coefficient is the inverse of the penetration depth.

As the modes are increasing in complexity there will be a higher penetration, since the maxima of the wave are closer to the border. But because as the intensity is calculated by the intensity at the boundary of the core and the cladding, this has no effect on expression 2.7.4 (as long as the added intensity at the boundary is taken into consideration).
When the intensity is high enough in the cladding, and there is a second waveguide close, light can "jump" from one waveguide to the other. This process has considerable losses. Because the electric field intensity is drastically lowered when it is not in the core. As in this thesis light is coupled into a ring resonator, therefore it is important to understand how much the intensity inside the second waveguide has been decreased. A short introduction to whispering gallery ring resonators is therefore added in Appendix B.

3. Procedure

In this chapter the set up will be described in depth to give the reader a clear view of the process used for measuring and imaging. First the procedure for the time-resolved paper experiment is discussed, after which the setup for the time-resolved whispering gallery mode resonator experiment are treated.

As a side note, in this chapter the words time and distance will be used for the same meaning, that is: The distance travelled by the light pulse. Because distance and time for the light pulse are the same. The terms can be used interchangeably.

3.1 Time-resolved transmission of paper experiment

As the pump laser pumps the Tsunami laser which is mode locked, there will be pulses emitted from the Tsunami with a refresh rate of 80.528 MHz. The width in time is 110 fs[12] . The output wavelength has a FWHM of 9 nm and the nominal power output is around 2 watts. This pulse will travel to an optical parametric oscillator which will up convert the wavelength of the pulse due to second harmonic generation. The output wavelength can be tuned between 1400 to 1600 nm by changing the temperature of the crystal where the difference frequency generation is occurring[11] and changing the length of the cavity inside the OPAL. In this set up it is 1550 nm (nominal output: 180mW) due to the compatibility of the used sum frequency generation crystal (BBO – Barium Borate) . The light from the OPAL has the same characteristics as the pulse coming from the Tsunami (most notably the pulse shape) but the polarization is changed from vertical[17] to horizontal. The up converted light is from now on called the gate beam. The residual coming out of the optical parametric oscillator is the non-used light in the difference frequency generation process, from here on out called the probe beam.

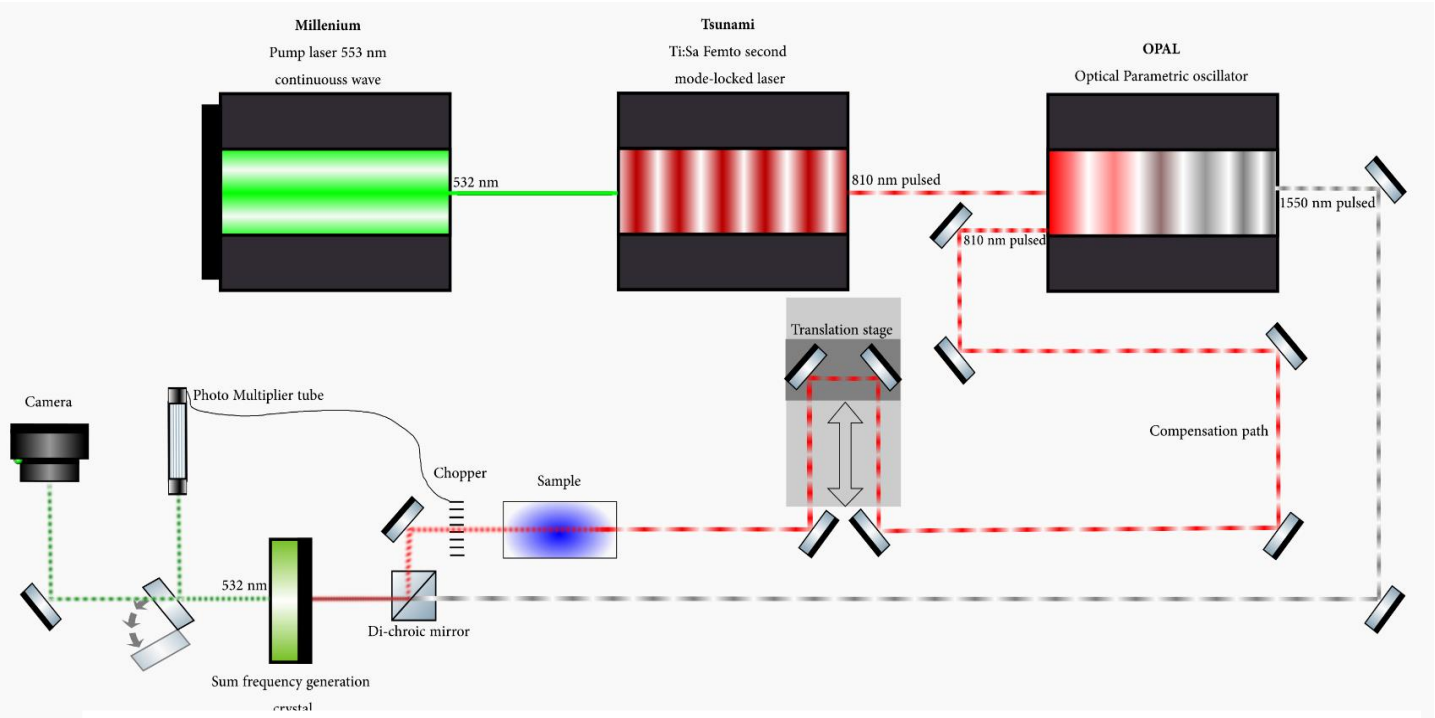

Figure 3.1, a schematic view of the setup. The dotted line is used to distinguish a continuous beam from a pulsed beam.

Before the sample there is a two lens system (not pictured in figure 3.1) to enlarge the beam width, which is done to let the beam hit a larger area of the paper and therefore a larger part of the crystal.

After the sample there is also a system of two lenses (not pictured) to image the sample onto the crystal.

In order to build the set up first the compensation of the probe beam has to be determined, because both pulses need to be travelling the same amount of time when they hit the SFG crystal. As the OPAL manual does not give an indication of the beam path length it is a matter of trial and error. The distance found so that the two pulses will converge at the SFG crystal and that the translation stage will be in the center of its path is 282±1 cm. Also in the compensation path is a polarization rotator, to ensure that both the probe and the gate beam are polarized in the same plane.

As is described in paragraph 2.3.1, the probe and gate beam enter the BBO crystal and where the two beams overlap temporally and spatially the pulse is up converted to a wavelength of 553 nm (calculated using expression 2.3.9).

To align and focus the setup a target is used that was manufactured by Thorlabs. This target is positioned in a holder on which the other samples will be mounted later on. The alignment and focusing of this target is of the utmost importance, as with for instance a paper sample it can't be tested if the focus is still optimal. So after the initial focusing with the target, the lenses will be fixed in their position.

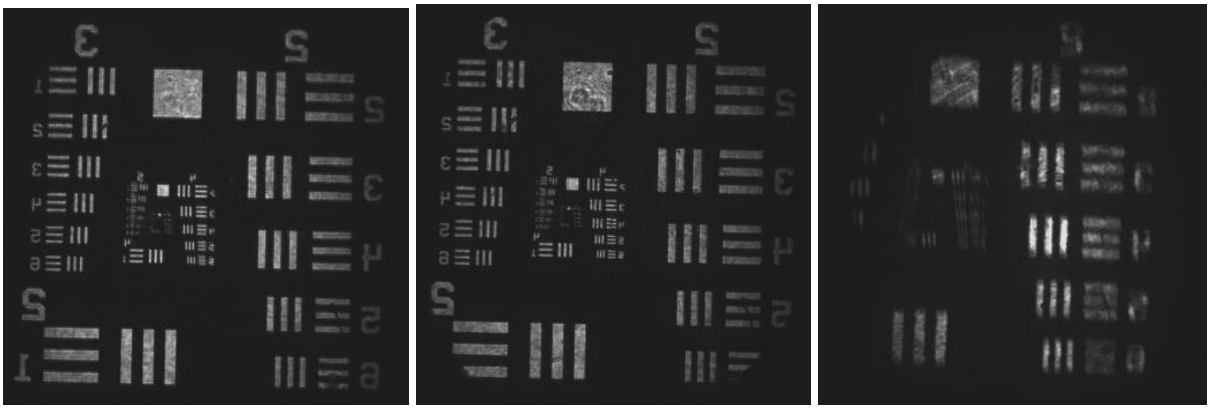

Figure 3.2, from left to right: The target with only the probe beam and no crystal,the non-time-resolved target with the BBO crystal (hence the cropping of the corners) and finally the time resolved image, where there is a degradation of the quality of the image visible.

In the second picture it is noticeable that there are certain defects in the picture (note, for example: the rings in the bright square) because of the imperfect nature of the BBO crystal. When the image is put into focus on the crystal the defects are shown. The intensity is also diminished, with the difference between the first and the second picture being one ND stop (which is a factor 10 lower). The last picture shows a very bad quality image; because of the up conversion of the wavelength, there is a negative effect on the vertical quality of the images because of the alignment of the lattices inside the crystal (some refraction occurs within the crystal itself). Along different angles in respect to these lattices different phase matching conditions apply, which leads to less light being up converted. This is the maximum quality images there is at the moment for this setup. A solution to this is added in the discussion.

Also a solution to this would be to find a thinner crystal, but this will decrease the output intensity due to a decrease of second harmonic generation because there is less volume the pulse is passing through.

The paper that has been chosen for the experiments is a normal piece of printer paper, First the piece of paper was placed under an electron microscope to see the structure, which is seen below.

Figure 3.3a, the side of the paper used in the measurements.

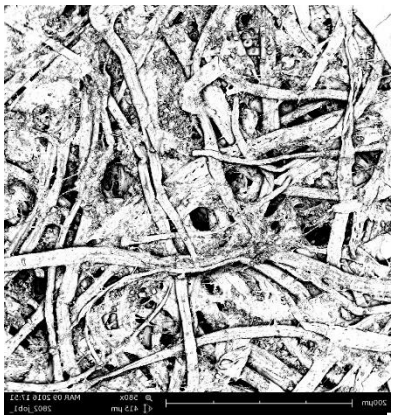

Figure 3.3b, an overview.

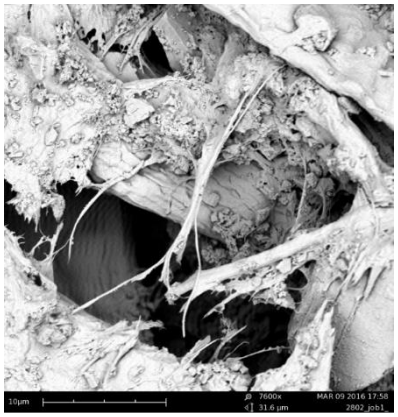

Figure 3.3c, a zoomed in picture of the structure.

As can be noticed, the paper is a chaotic assembly of fibers glued together. The paper itself is not a complete flat surface, which is also indicated in figure 3.3c on the right. This image is zoomed in on a hole of ~12 um wide.

After the different parts of the setup are aligned and focused the target is replaced by a sample that is made of normal copy paper (0,1 mm thick, measured in paragraph 5.2). First the start of the pulse is searched. When this starting point is found the translation stage is moved backwards by 600 femtoseconds. The measurement is started by using a labview program, which will move the translation stage with increments of 5 μm which corresponds to 33 femtoseconds. The dwell-time (the time the photo multiplier tube is measuring per position) is 2 milliseconds.

To switch between the PMT and the camera a flip mirror was installed to let the light go through to the camera. The camera is an ANDOR M912 camera. This extremely sensitive camera is cooled to minus 40 degrees. This is done to decrease the noise made by dark current. As the intensity is decreasing due to further moving through time, the exposure time(dwell-time) is increased, from 2 seconds to 40 seconds. The different exposure times by the camera are noted below the images.

3.2 Time-resolved transmission of a waveguide experiment

As part of the upgrade to the setup a new SFG crystal is used. This crystal is a BIBO crystal of 0,5 mm thickness, it is expected that there would be an increase in spatial resolution due to the decrease of thickness. The BBO crystal used before had a thickness of 2 mm. A better understanding of why a BiBO crystal is a better candidate for these kind of measurements than the BBO crystal can be found in the supplementary article published in the journal: Light: Science & Applications (Nature publishing group) by MSc. L. Pattelli[18]. As the focus of this thesis is more on the setup, its results will not be discussed. In Appendix A there will be a small research to the expected increase in spatial resolution.

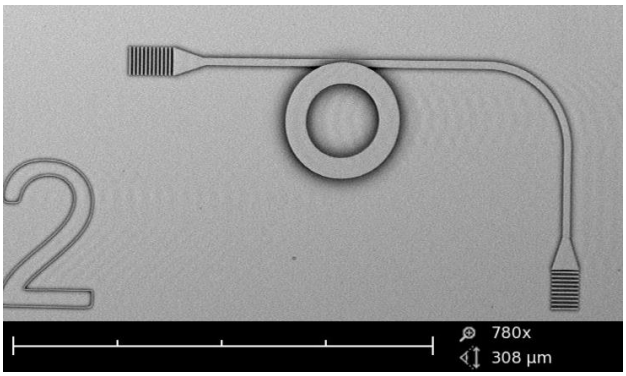

Figure 3.4, a SEM image of the waveguide with the WGMR attached to it.

To get the light inside the whispering gallery mode resonator a waveguide with an in and output coupler was fabricated by MSc. Sara Nocentini with a direct laser writing 3D lithography system (Nanoscribe GmbH). The left square with stripes is the input coupler, the square on the right is the output coupler. The waveguide itself is 2,5 µm wide and 2 µm tall. The resonator stands off the ground by 2,2 µm so a gap of 200nm is present. The resonator itself has an outer radius of 20 µm and an inner radius of 11 µm. The waveguide is horizontally 100 µm long till the beginning of the curve and from the curve vertically 10 µm. The radius of the curve is 30 µm, after the curve is another 30 µm and the triangular shape at both the couplers is 10 µm long. The effective refractive index of the material (IPDIP) of the waveguide and resonator is 1,525±0,0005.

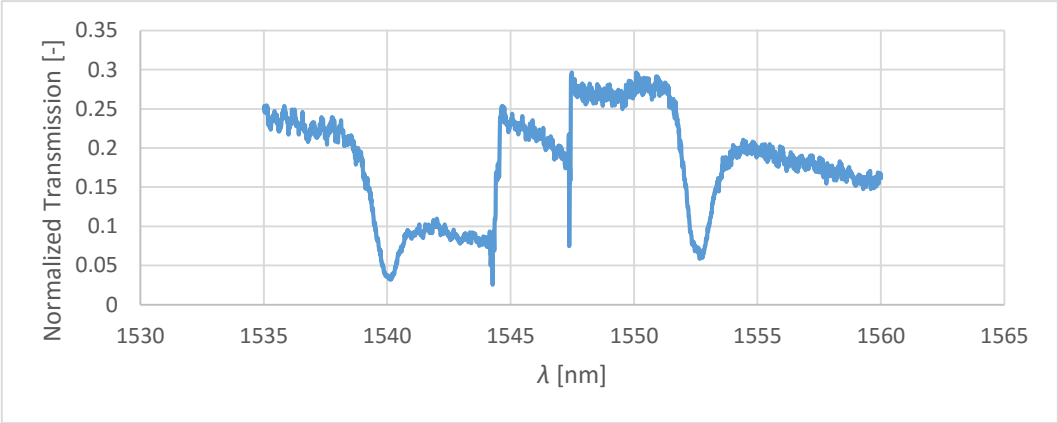

Figure 3.5, the transmission of the whispering gallery mode resonator.

To try and couple light into the coupler first a measurement of the response of the waveguide was conducted with the whispering gallery mode resonator attached to it to see which wavelength would be most suitable for this research. As the losses are quite high for such a waveguide the most optimal wavelength should be chosen. The fabrication and transmission measurement of this sample was carried out by MSc. Sara Nocentini. She researches tunable WGMR's, and has lent this project one of her samples.

The conclusion from figure 3.5 is that the wave couplers of the waveguides are optimized for a wavelength of 1550nm. As the beam that is previously used as the gate beam is of that wavelength, the probe and gate beam are interchanged. The losses at the input and output coupler are approximately 95%. For this reason, the probe beam is focused with an objective with a magnification of 10x to ensure maximum intensity is focused on the input coupler.

To collect the maximum amount of light from the output coupler an objective with a magnification of 50x is used. The use of two objectives will degrade the temporal resolution as the objectives consists of multiple lenses which will scatter an amount of light. This influence will be discussed in paragraph 4.3.2.

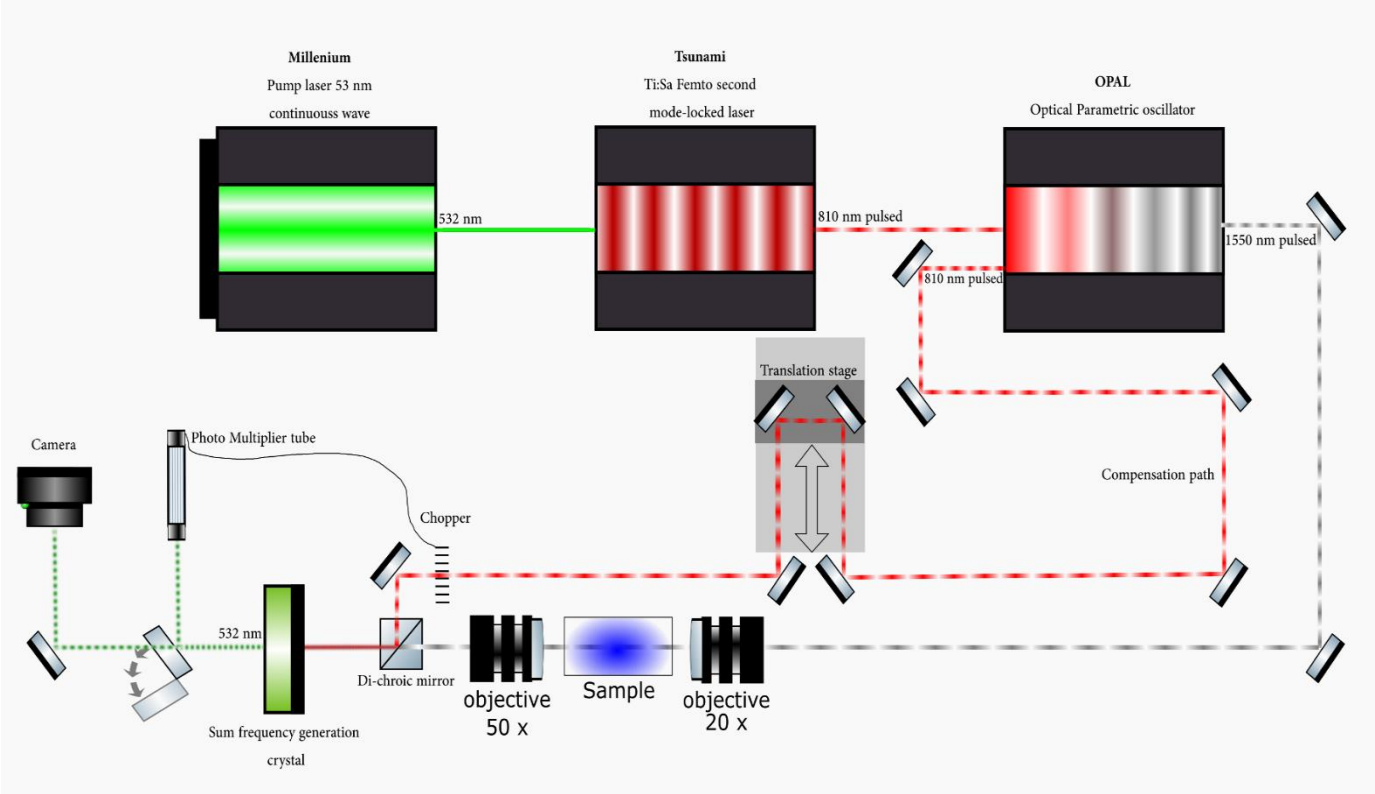

Figure 3.6, a schematic view of the for the whispering gallery mode resonator measurements.

For the input of the probe beam the objective is first aligned with the input coupler. This alignment is not carried out with laser light but with a desk light because the output with laser light is IR light, and the camera is not susceptible for this wavelength. It is possible to illuminate the sample and aim it with a time-resolved beam, but the resolution is too low to aim it properly.

Noted is that for the input coupler alignment there has not been a picture made with white light because the white light exposure was only thought of later. By that time the input objective was already aimed correctly and did not need any further adjustment.

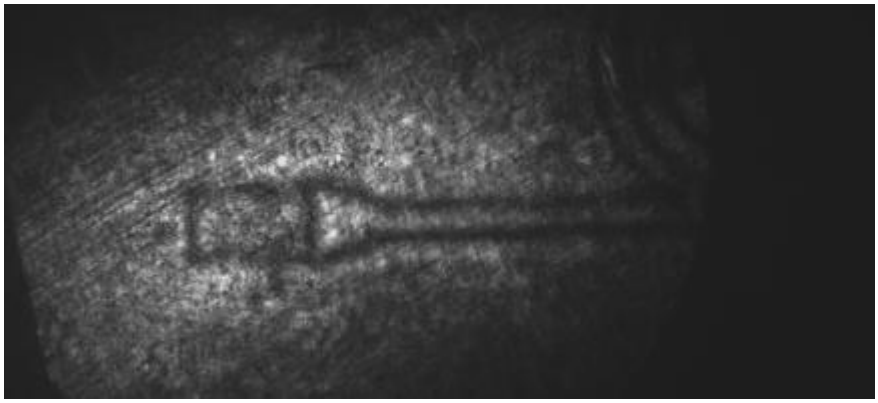

Figure 3.7, example of the input coupler alignment with Time-resolved exposure.

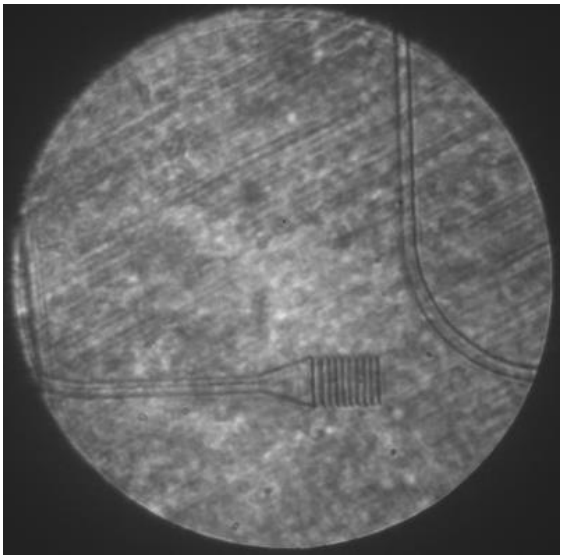

Figure 3.8, example of the output coupler alignment with a white light exposure.

The positioning and alignment of the input objective is verified by making one image when the output objective is in the same axis as the input objective, this to verify everything is well aligned.

Two measurements were carried out the first one measuring the input signal. This is where the collecting objective is on axis with the input objective. After this measurement white light is shown in to the input objective, illuminating the whole sample. The camera is put on live view (low quality) and the output objective is moved to the position showed in figure 3.8. This means that the two objective are not on the same axis anymore, but as the light is moved from the input coupler to the output coupler this is necessary.

In figure 3.9 the two different positions of the collecting objective coupler are shown. The pulse is travelling from the top of the images downwards, first hitting the glass substrate before interacting with the coupler.

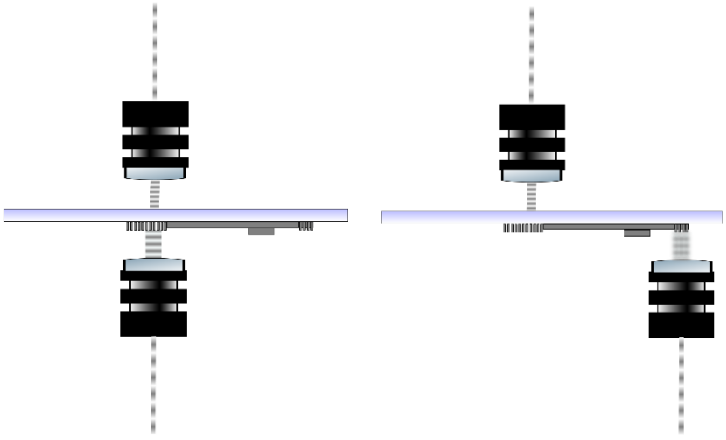

Figure 5.7, a top down view of the time-resolved measurements done on the waveguide assembly. Left the input coupler measurement, right the output coupler.

4. Accuracy

4.1 Photo multiplier tube

In the time resolved measurements used in this thesis the probe beam is interrupted by a chopper with a frequency of 20 Hz. This allows the estimation of the error in the Photo Multiplier Tube coming from the dark current and stray light in the lab. Although the last one is kept to a minimum (in order to achieve this, the PMT was built inside a box), there is still some light entering the tube.

Because the probe beam is interrupted, there will be no light up converted by the SFG crystal. The PMT will still give a count, which is retracted from the signal which is measured when the probe beam is not chopped. The following formula is used to determine the actual counts.

$$N_c = \sqrt{N_s^{\,2} + N_d^{\,2}} \qquad (4.1.1)$$

Where:

N_c	=	corrected count	[-]
N_s	=	signal count	[-]
N_d	=	interrupted count	[-]

This calculation is done by an SR-400 Photon counter where the output is connected to a computer running a labview program. The output of the photon counter is only N_c which implies that it is impossible to do this calculation manually because the signal count and interrupted count are not able to be extracted from the photon counter.

Expanding on the already correct N_c, a statistical error in the was data found. As stated by Hudson[19], for a normally distributed system the standard dispersion (noise in the signal itself) of N_c around its mean is given by the square root of the value of N_c. To ascertain that the results stay in the given accuracy, the graphs will be given error bars of 3 times the standard deviation. This will give an accuracy of 99,75%[19], meaning that in 99,75% of the cases the data found will be within the boundaries of the given accuracy. Although the uncertainty is expected to be lower and can be calculated by repeating the given experiments a set number of times, calculating from the standard deviation a maximum deviation. Time limitations resulting from the breakdown of the pump laser and optical parametric oscillator.

4.2 Temporal uncertainty

The temporal uncertainty is given by the uncertainty of the position in the translation stage. From the producer of the stage (Thorlabs[20]) it is concluded that the translation stage uncertainty is 1 μm, the uncertainty contributed by this in time is given by the following formula:

$$\Delta t = \frac{1 \cdot 10^{-6}\,\mathrm{m}}{2{,}99 \cdot 10^{8}\,\mathrm{m \cdot s^{-1}}} = 3{,}3\ \mathrm{fs} \qquad (4.2.1)$$

This number should be multiplied by two, since as the light beam moves both up and down the translation stage. In addition, because as the translation stage is controlled by a stepper motor, it is unclear if the uncertainty is still 1 μm or lower than this number when this is always moving in the same direction.

This gives an extremely low value for the temporal accuracy. with the inaccuracy of the translation stage this gives a temporal inaccuracy of 6,6 fs.

A better solution to determine the temporal accuracy would be to execute multiple measurements of the same sample. As the position of the peaks have to be the same for every measurement, a standard deviation can be calculated. This solution is also added as a to-do in the discussion at the end of the thesis. As it is shown in the following paragraph that this is a very low inaccuracy, it will not be shown in the graphs.

4.3 Temporal resolution

This chapter will first discuss the time resolved experiment with paper is discussed, after which the Whispering gallery mode resonator experiment is treated.

4.3.1 Time-resolved paper experiment

Besides the inaccuracy of the translation stage there is another way of looking at the temporal accuracy of the setup. This is to look at the intensity distribution of the incoming pulse[21]. When the pulse was created in the Tsunami mode-locked laser it is assumed that it has a Gaussian intensity distribution. The difference between a perfect Gaussian distribution and the signal pulse measured by the PMT can be calculated, which will reveal the change in intensity distribution. How much it defers from a Gaussian distribution is in direct correlation with the quality of the setup. If the signal is degraded in any way, the R^2 value will be low. Of course this correlation has to be performed without a sample or optics present, for this will surely shift the intensity distribution due to multiple scattering inside the sample and the optics used.

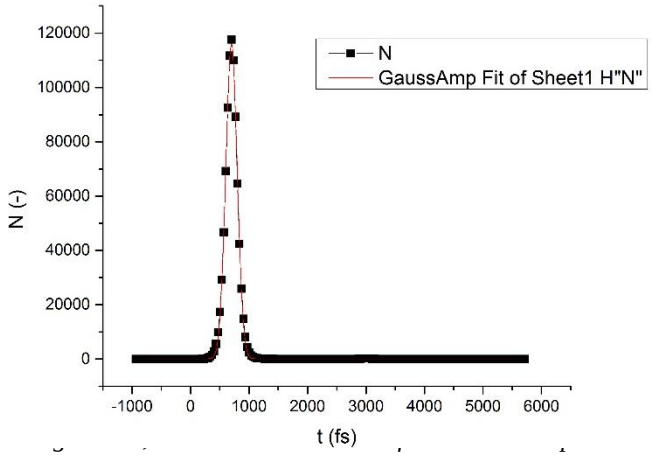

without any optics versus a perfect Gaussian dispersion.

Table 1, values of statistical analysis of the cross correlation.

	Value	Standard Error
A	$1{,}16 \cdot 10^5$	$3 \cdot 10^3$
FWHM	230	1
R^2	0,99917	-

From this analysis it can be concluded that the temporal resolution would be the same as the full width halve maximum calculated with above method, the value of the FWHM is 230±1 fs. This is the time that the gate is open. Unfortunately, it is not certain that this number represents the absolute temporal precision, because: By the addition of optics in the optical path of both the signal and gate beam will cause a shift in the distribution of the intensity, even badly aligned mirrors or lenses could give backscattering and multiple internal reflections, resulting in multiple peaks. Also realigning the optics would render this analysis invalid, and a new cross correlation would need to be performed every time something changes in the setup. Even temperature would be an issue, as the output of the Tsunami and the OPAL apparatuses are very sensitive to shifts in temperature in the lab.

4.3.2 Time-resolved transmission of a waveguide assembly

For the experiment of the WGMR a new crystal (BiBO) and two objectives are added. Because these objectives have multiple lenses, light will take a longer time to travel through these objectives as they are dense. It is believed that the temporal resolution will decrease due to the addition of these two objectives. The same cross correlation as in the previous paragraph is carried out with the exception that the intensity of the pulse is 2,5 times higher, as the objectives focus the light better unto the SFG-crystal.

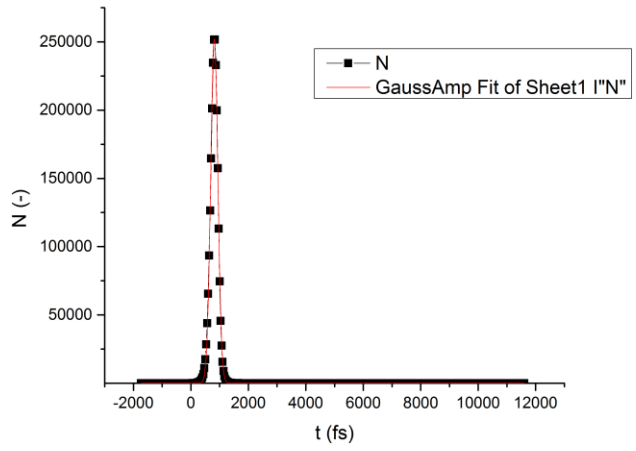

Figure 4.2, the cross correlation of the measured pulse with two objectives versus a perfect Gaussian dispersion.

Table 2, values of statistical analysis of the cross correlation with the addition of two objectives.

	Value	Standard Error
A	$2{,}52 \cdot 10^5$	$5 \cdot 10^3$
FWHM	320	1
R^2	0,9988	-

As the FWHM is increased by 90 femtoseconds, it is clear that some resolution is lost. This decrease is necessary due to the small nature of the in and out couplers and the need to focus the light onto this very small object. Regretfully there is not a cross convolution of only the new crystal, as this would enable a direct comparison between the BBO and BiBO crystal. As the pump laser and the Opal are under repairs, it is not possible to do so until these machines are in working order. This measurement is added to the suggestions chapter.

4.4 Calculating transport mean free path

Before calculating the transport mean free path different variables have to be calculated, here is a short description of their uncertainties.

For equation 2.6.11 there is still the need to find the thickness of one paper sheet. This is done by using a precision caliper (uncertainty 1 mm) and measuring the thickness of N_p = 500 sheets of paper (a guessed uncertainty is 1). The thickness of the pack of sheets is: d = 51±1 mm. The uncertainty in the measurement of the thickness of paper using the method dictated by[22]:

$$\Delta L = \left(\frac{\Delta d}{d} + \frac{\Delta N_p}{N_p} \right) \cdot L = \left(\frac{1}{51} + \frac{1}{500} \right) \cdot 102\ \mu\text{m} = 2{,}2\ \mu\text{m} \qquad (4.4.2)$$

So the definitive thickness of one sheet of paper used in the experiments is 102 ± 2 μm.

As *A(n)* is calculated by using a polynomial fit with an uncertainty far below 0,05%[15]. The uncertainty of *A(n)* is not used in the calculation of the Transport mean free path.

To find the uncertainty in the answer of l_t is difficult, since the answer is approximated. The author has made the decision to calculate all the different answers with a minimum or maximum of their own uncertainties, and consequently take the maximum deviation as the uncertainty in the answer. Because there are 3^3 times possibilities in this process a program was written to quickly find the maximum. The rule for this program is that it cannot have an imaginary or negative answer. The code can be found in appendix D.

5. Results

In this chapter the results of the measurements will be presented and discussed.

5.1 Cross convolution comparison

When the translation stage scans through the moment the two pulses overlap at the SFG crystal the intensity that is being up converted is directly proportional to the amount of overlap the two pulses have, both spatially and temporal. It is the integral of the overlap of the two pulses.

To see the difference in quality of building the setup in comparison to the setup in 2012, the two measurements are compared against each other. Note: The power of the pump laser was higher in 2012 than it was while the cross convolution was made with the new setup (10 watts against 8,2 watts). It is expected that this will have a negative effect on the cross convolution.

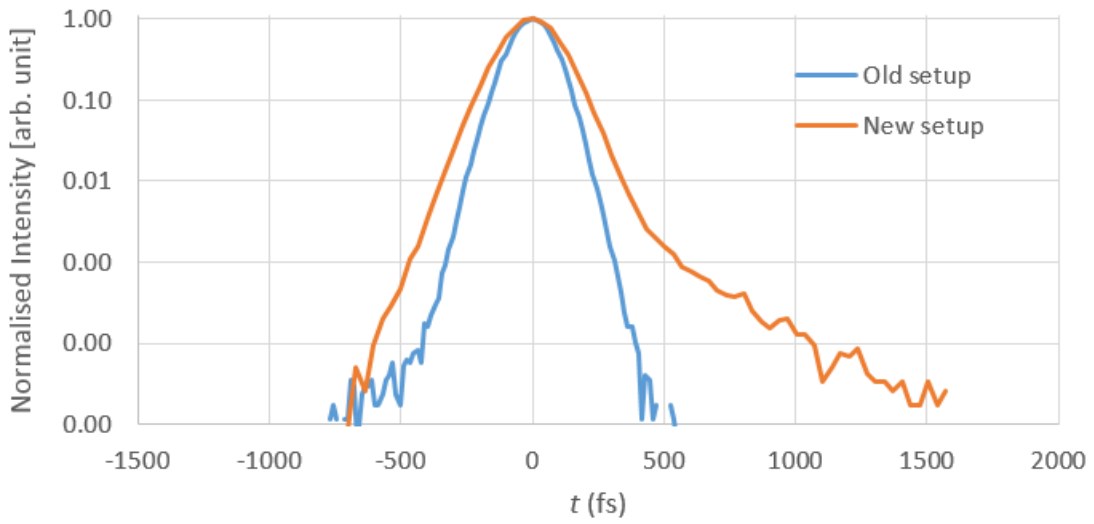

Figure 5.1, The comparison of the cross convolution of the old and new setup. The Y-axis is logarithmic.

Looking at figure 5.1, it is clear that the new setup has an unevenly distributed gate opening time (as the left part of the pulse is much steeper than the right part). This gives rise to the thought that there is something in the setup that is scattering light. Mirrors with dust particles or lenses that are not well aligned can give TIR, the implications of which are unknown, as there is no study on this particular subject. For this thesis it is enough to say that the temporal accuracy has deteriorated. But the significance of this is less than figure 5.1 dictates: The gating times are well below one picosecond (one tenth) and the closing part of the gate still has a shorter decay time than that are taken place (paper).

The cause of this can be the loss of power from the pump laser, which has a non-linear effect on the output power of both the Tsunami and the OPAL. It can also be the conditions in the lab itself, as a change in temperature, air speed, humidity or even dust particle density in air has an influence on the light travelling speed (which is measurable in this system).

5.2 Time-resolved paper experiment

For this experiment a step distance of the translation stage is selected of 5 µm and a dwell time of 2 milliseconds, this means that for every step the PMT measures for 2 milliseconds. 5 µm corresponds to a time of 33,44 femtoseconds, which is small enough for the expected decay time. The origin of coordinates on the x-axis is chosen by the author himself, this position is arbitrary, it has been chosen to put this sometime before the main event. This is why there are data points in the negative timescale.

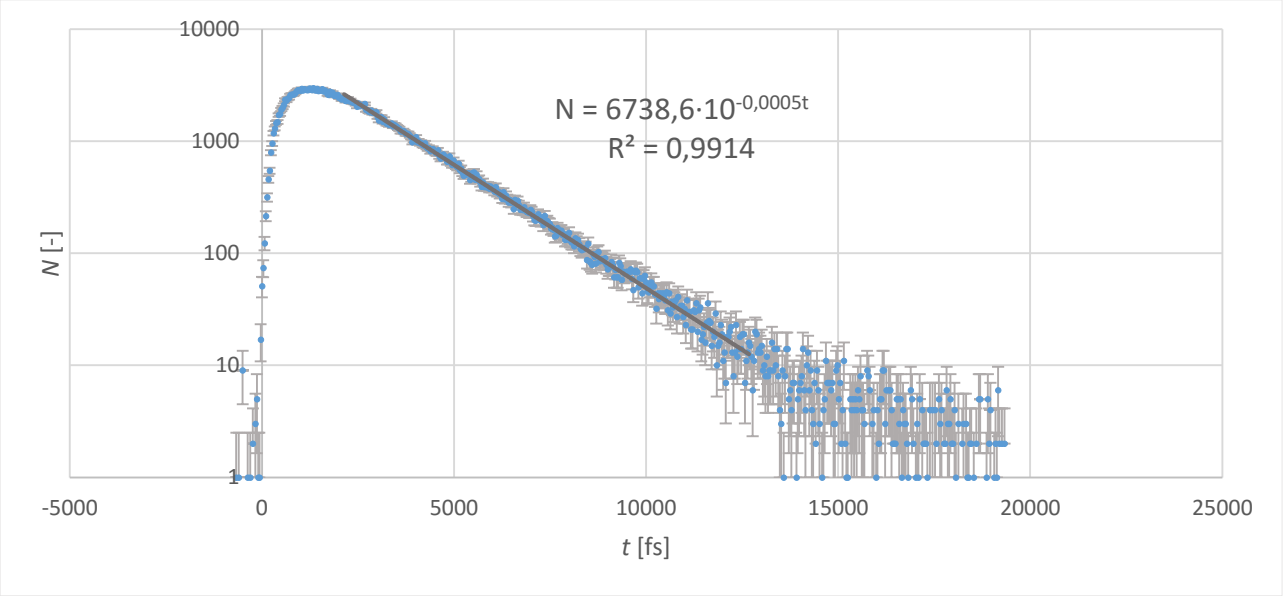

Figure 5.2, the time resolved paper measurement.

As can be seen in figure 5.2, the inaccuracy is very high at the moment that the intensity drops below 10 counts. The curve makes an exponential decrease after the initial hit of the pulse. The τ found here will later be used for the calculations of the transport mean free path.

To further increase the accuracy of the setup as well as measuring the light scattering longer through the paper an increase of the dwell time is recommended. Also, to further enlarge the dynamic contrast of the setup, an ND filter can be used in the first more intense part of the pulse. When later the intensity is low enough, the experiment is stopped, the ND filter is removed and the measurement can continue from the same point. After the measurement is done, the data can simply be manipulated in a software suite of choice to manually heighten the intensity when the ND filter was installed. This gives a factor ten higher maximum input for every ND filter used.

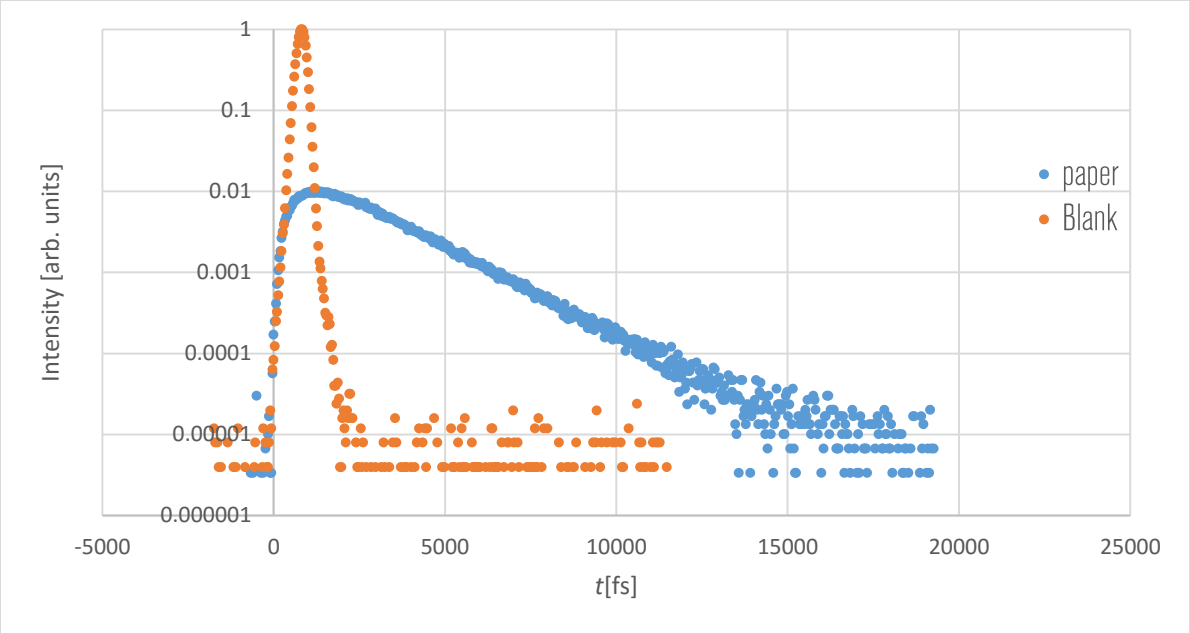

Figure 5.3, the comparison between the pulse without a paper sample(orange) and with a paper sample(blue). The Y-axis is logarithmic; the values are normalized.

Figure 5.3 is made to give a comparison of a pulse going through the setup without encountering paper and with this encounter. It is interesting to see in the above figure that the initial increase (rising of the peak) in intensity is the same. From this it is concluded that some of the photons do not interact with the paper at all and ballistically go through the paper. When the pulse has reached its top it is seen that the paper has a much slower decrease of intensity. This is contributed by the scattering of the photons inside the paper, which takes more time. The photons will thus exit the paper later.

The images taken with the camera are shown below, the standard exposure time for the camera is 20 milliseconds, unless otherwise stated.

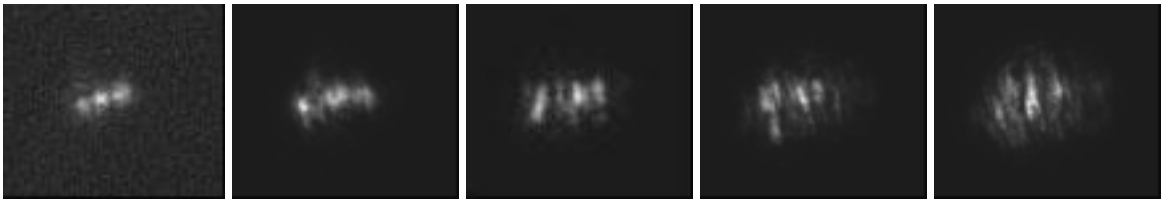

-334 fs (exp: 5 sec) 0 668 fs 1337 fs 2005 fs

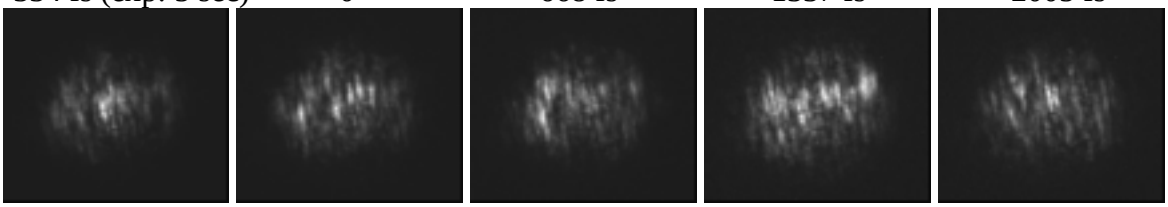

2637 fs 3341 fs 4009 fs 4677 fs 5345 fs

The second row has an increased exposure time of one second.

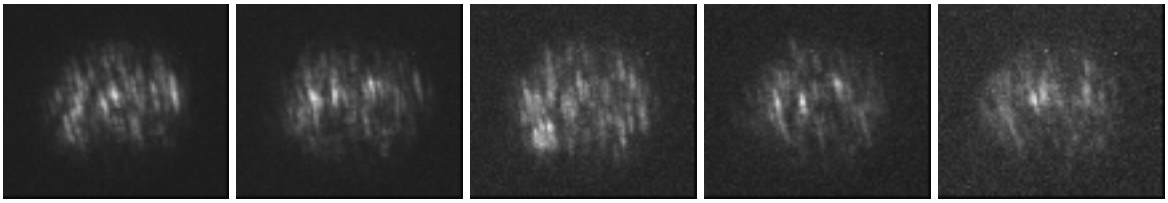

6013 fs (exp:2 sec) 6681 fs (exp: 4 sec) 7349 fs (exp: 8 sec) 8017 fs (exp: 8 sec) 8685 fs (exp: 20 sec)

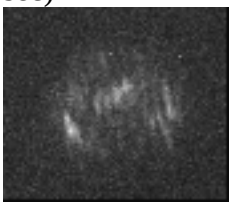

9353 fs (exp: 40 sec)

Figure 5.4, the assemble of time-resolved images.

If the zero point of impact is compared to later (+5000 fs) images it is clearly seen that light spreads evenly in a circular shape in the paper. This is predicted by the theory that the light will scatter randomly in every direction with a certain average step length. The stripes that are present are not identified. An explanation can be that these are lower situated cavities in the paper as in figure 3.3c. Or These were originally point sources, but the SFG crystal smears them out somewhat in the vertical direction. For this the term “time-resolved speckle” is introduced.
A suggestion made by MSc. Pattelli is to increase the exposure time drastically and make two images per position in time. The first would be the image with the signal beam, while the second would be the same image, but the signal beam would be blocked manually. When later these two image are subtracted from each other there would be a decrease in noise coming from the camera sensor (as seen in the 9353 fs image). The camera uses a bias voltage to keep electrons inside a quantum well. This bias voltage has some jitter, which causes electrons to go out of the quantum well, and the camera registers this as a change in intensity at that specific pixel.

5.2.1 Calculating transport mean free path

To calculate the transport mean free path, a numerical solver needs to be used. As the answer is a numerical solution to a problem that cannot be solved analytically, this solver is constructed in a Matlab program created by the author using the VPAsolver inside Matlab. This solver is a quite brute force solver as it just tries to find a number where the equation is correct (to a certain uncertainty). This number (or numbers) it finds will still be an approximation, but the amount of accuracy is far greater than the uncertainty that is given for the other variables in the equation. For equation 2.6.11 there is still the need to find the thickness of one paper sheet. Using the already named variables for the measurement of paper thickness in paragraph 4.4, the slab thickness (*L)* would be:

$$L = \frac{51 \cdot 10^{-3}}{500} = 102 \pm 2 \ \mu\text{m} \qquad (5.2.1)$$

The τ is calculated from the same data as figure 5.2, but this time the program origin is used because, Excel does not give exact answers. The same starting point is used for the fitting of the trendline, but it ends somewhat earlier, as the noise in the data from 12 ps is degrading the approximation.

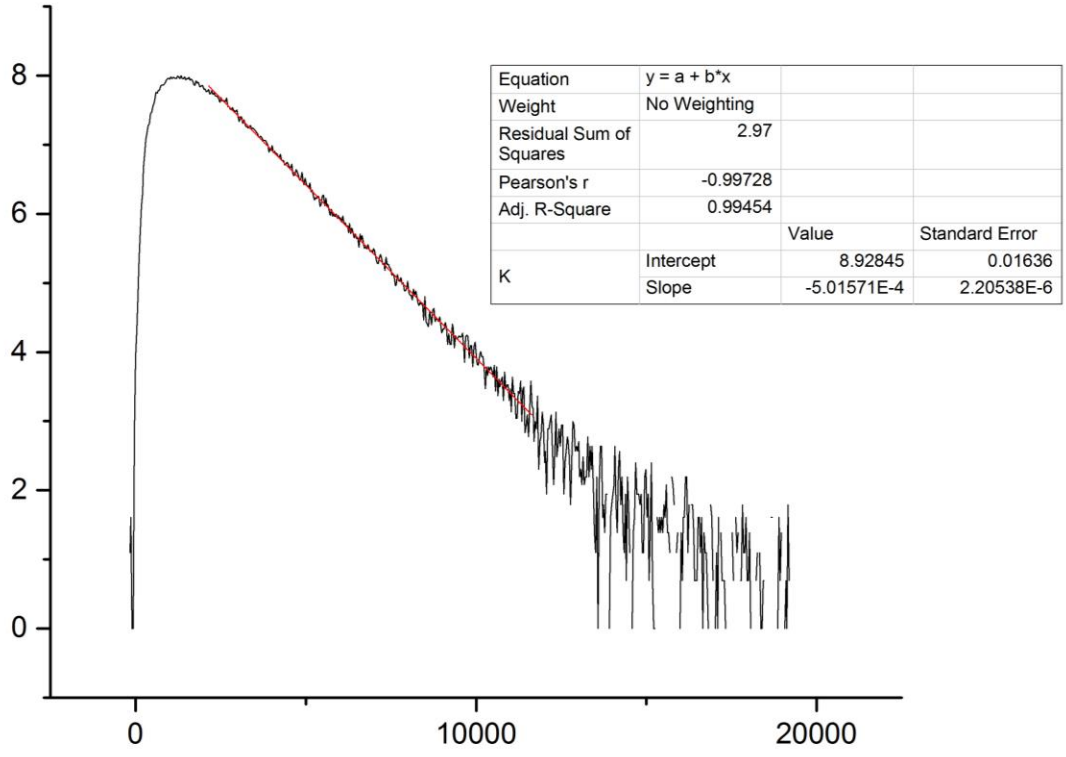

Figure 5.5, the extrapolated tau data, the y-axis is in log scale with base number e.

The τ found in figure 5.4 is: 1990 ± 10 fs^{-1}.

Using a slightly lower refractive index than that of cellulose (n = 1,5) seems like a logical step because the paper is not completely filled cellulose, but multiple stripes and layers of cellulose glued together. This is supported by Pattelli's thesis[23] as he calculated the refractive index of paper by using the filling fraction of paper. Because of this, the refractive index is chosen to be 1.4 with a large uncertainty of 0.05.

The function *A(n)* is calculated using the polynomial approximation, found here[15]:

$$A(n) = 504.332889 - 2641.00214 \cdot 1,4 + 5923.699064 \cdot 1,4^2 - 7376.355814 \cdot 1,4^3 ... \\ +5507.53041 \cdot 1,4^4 - 2463.357945 \cdot 1,4^5 + 610.956547 \cdot 1,4^6 - 64.8047 \cdot 1,4^7 = 2,95 \quad (5.2.2)$$

When all the individual variables for expression 2.6.11 are calculated, they can be inserted into the formula:

$$1990 \cdot 10^{-15} = \frac{\left(102 \cdot 10^{-6} + 4/3 \cdot 2,97 \cdot l_t\right)^2}{1/3 \cdot l_t \cdot \frac{2,99 \cdot 10^8}{1,4} \cdot \pi^2} \quad (5.2.3)$$

The exact result from the solver is: $l_t = 19,5 \pm 4,8$ μm, which, taking inconsideration the uncertainty is: : $l_t = 20 \pm 5$ μm .

This is slightly higher than MSc. Pattelli found in 2012 ($12,7 \pm 0,5$ μm[23]). This can be because the paper used in the 2012 experiments is slighty thicker (114 μm) and of a different quality, a denser type of paper would explain the shorter length to fully isotropic scattering events.

The uncertainty is large; this is because the uncertainties of the variables is quite high, and expected to be more pessimistic than the reality is. A better way of determining the right uncertainty would be taking more measurements. Using the statistical outcome of a multitude of measurements would give a more exact uncertainty, because now the uncertainty is the maximum uncertainty possible with the given variables and their known uncertainties.

5.3 Time-resolved transmission of a waveguide assembly

For the measurements discussed in this paragraph the dwell time is increased to 4 ms and the step length is 1 μm.

As the whispering gallery mode resonator assembly is built on a glass substrate, it is interesting to see if there are reflections and scattering that can be measured at the input coupler. For this measurement the two objectives were still in alignment, for the output coupler the output objective is moved (as stated in paragraph 3.2). The beam first goes through the glass before hitting the input coupler. The pulse is first entering the glass substrate. After this it will interact with the input coupler, the collection objective is on axis with the input objective.

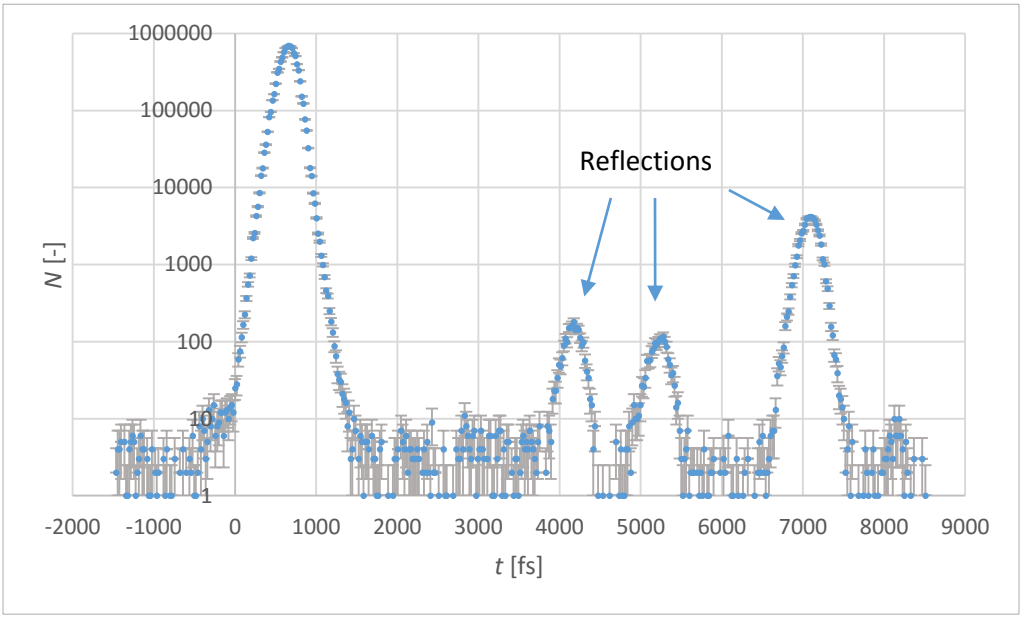

Figure 5.6, the time-resolved measurement of the input coupler. The left peak is the main probe pulse, while the remaining pulses are reflections of the in coupler structure and glass.

The reflections are caused by light that is entering the glass substrate and refracting at the boundary of the waveguide assembly. As the time between the main pulse and the reflections is too long for internal reflections inside the waveguide caused by the output coupler (going to the output coupler and reflect of the final boundary back through the waveguide) then this expected reflection would be. This reflection from the waveguide would be expected after a 1000 femtoseconds after the initial pulse.

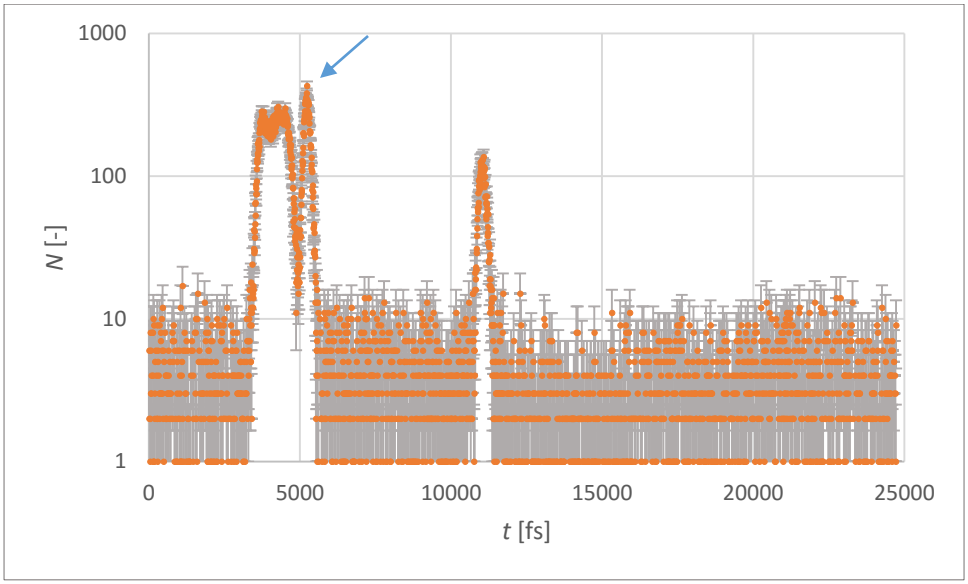

Figure 5.7, the time-resolved measurement of the output coupler, the arrow denotes the peak where the images are made.

Now the collecting objective is moved to the position where it can collect light from the output coupler, as discussed in paragraph 3.2.

The starting point for the measurement of the output coupler is 10 ps later than the start of the input coupler measurement, because there was no light coming out of the output coupler before this point. For figure 5.7 this means that it should shift to the right by 10 ps. And here is a problem. The pulse that is entering the output coupler is arriving too late from the output coupler, as the light is traveling with a speed of $1{,}96\cdot10^{8}$ m·s^{-1}[§§§] (using expression 2.1.5) through the waveguide. If the pulse would not interact with the resonator it should take (adding all the lengths of the waveguide together from chapter 3):

$$t=\frac{\left(10+100+\frac{2\pi 30}{4}+30+10\right)\cdot10^{-6}}{1{,}96\cdot10^{8}}=1010\pm7\text{ fs} \qquad (5.3.1)$$

This is 9 picoseconds earlier than measured. It is possible the light interacted with the resonator, and made a few roundtrips. One roundtrips equals to:

$$t=\frac{2\pi 20\cdot10^{-6}}{1{,}96\cdot10^{8}}=640\pm7\text{ fs} \qquad (5.3.2)$$

As the time difference between the main peak from the input coupler and the highest peak from the output coupler is 12,99 ps, it could have taken ±19 (18,72) roundtrips in the resonator. This, however, is a mere guess, and is not a very likely one since as the resonator used in the experiments is not of that high quality (see appendix B for an approximation of the photon lifetime inside the resonator). It also does not explain the other peaks. Although it could perhaps be said that simply

[§§§] The uncertainty is not named as it is $3\cdot10^{-4}$ m·s^{-1}. For this it is not employed in the calculations.

adding more roundtrips in the resonator gives the later peak at 21 ps. it does not explain the broad two peaks, as the time between these two peaks does not correspond with the roundtrip time of the resonator.

It could be that the light speed inside the waveguide assembly is not correct. But the refractive index of IPDIP (the material the waveguide is made from) has been measured by MSc Sara Nocentini and is proven to be correct.

There are more experiments necessary to explain this delayed output from this waveguide. A suggestion is to use the same waveguide without the resonator, so that it cannot influence the time inside the assembly. Also a straight waveguide without a bend would be an interesting experiment, to exclude the possibility that light is reflected inside the bend of the waveguide. Furthermore, there is a possibility that the light is trapped inside the boundaries of the couplers themselves. As the assembly is not manufactured in one piece, there is a slight gap between the waveguide and couplers, but this is not a very likely cause of the problem, as the losses inside the assembly are extreme. These suggestions are added in the chapter 7.

As with the paper experiment time-resolved images are made. the peak that is chosen to image is the highest peak in figure 5.7, around 4000 fs (denoted with an arrow). The image sequence starts at the dip of 10 counts, all the way up to the peak of 400 counts. The images are made by superimposing figure 3.8 (the white light aiming image) on the time-resolved image that is measured. The fil rate (amount of overlay of the measurement image is 82%) the time of imaging

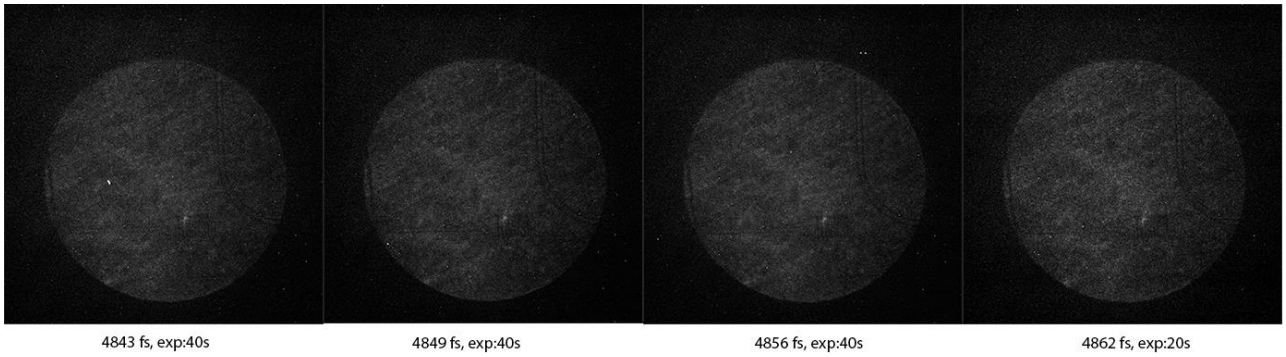

Figure 5.8a, the first part of the images taken of the output coupler.

is shown under the images. All the images have had the same software editing done to enhance the image, as the light output is too low when the images are super positioned on the white light image (the software editing is shifting the levels and increasing contrast). As there was no difference to be seen, the step size is increased in the second part of the sequence. The superimposing of two images is done to give the reader a sense of direction and size.

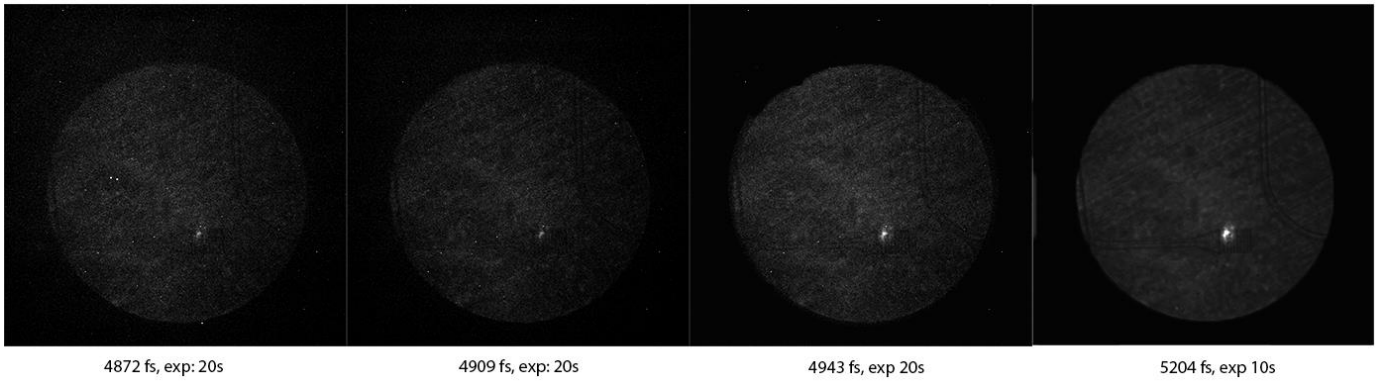

Figure 5.8b, the second part of the images taken of the output coupler.

In figure 5.8b, it is definitely possible to see a light spot. That gradually grows in intensity. Even when the exposure time is decreased by half. A zoomed in picture of this with a superimposed background is shown in figure 5.9.

It is observed in figure 5.9, the output is not coupled outwards in the middle but on the side of the coupler, and no coupling of light happens in the later barriers.

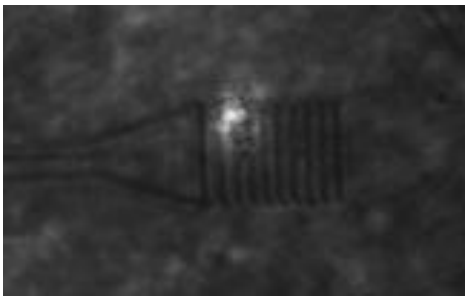

Figure 5.9, the 5204 fs image zoomed

As there are multiple ways these images could be enhanced, with the already explained subtracting dark images method. it is concluded that time resolved imaging of a whispering gallery mode with an attached assembly of input and output couplers is possible. This opens up a lot of possibilities for further study, for example to increase the efficiency of input couplers, as the pulse intensity can be imaged in detail.

6. Conclusion

The answer to the first research question: “What is the temporal accuracy of the rebuilt setup?” is in short 320 fs. If the comparison is made with the older setup of 2012 it is 90 fs longer than it used to be. The importance of this is debated: as the decay times of the samples that are being measured are lot longer than 90 fs, the negative influence from this is negligible. Furthermore, there are no data on whether the sum frequency generation crystals have a different decay time. The change to another crystal can influence the open-gate time drastically, as the decay times can differ from the crystal used in the cross convolution measurements in this thesis.

With paper there is strong evidence that a part of the pulse is not interacting with the paper at all, and just ballistically shooting through the paper. The decaying of the intensity is a lot longer with paper than without (as expected). The transport mean free path is longer than the measurement in 2012. Since the transport mean free path is heavily dependent on the properties of the medium that is being researched it is assumed that the difference in the paper sheet is the cause of this. The uncertainty in the answer is high, mainly because the refractive index of paper is not calculated but assumed, and therefore a large uncertainty is assumed. When the refractive index of paper is determined the uncertainty will be lower, and when this is inputted into the solver program the uncertainty in the answer will be much lower still.

The images show a circular outward movement from the initial pulse onward, as expected by the theory (bell-shaped intensity shape). Where the time-resolved speckles are coming from is still a question that can be researched, as there are no images of paper with the new crystal. It will be interesting to see if this phenomenon is still visible.

To answer the last question, the setup proves that it is sensitive enough for the low output of a waveguide assembly, but to investigate the output signal coming from the waveguide assembly with a resonator attached to it is not possible. Why the pulse and resonances are exiting the output coupler this late is not known, as the different resonances do not fit to any length of the waveguide or photon lifetime inside the resonator. The identification of the peaks cannot be done without further measurements of different arrangements to allot the different peaks to their source.

The imaging of the output coupler is possible albeit barely. The noise that is caused by the shutter being open that long almost drowns out the signal (especially in the lower intensity regions of the peak). A solution besides enhancing the images with the use of software is given in the form of making a dark image before or after the image is made.

This is at the moment the first time it is possible to perform time resolved imaging of a waveguide in a wide-field arrangement (time-resolved setups exists where a fiber is positioned just above a sample, where it can “image” by measuring every pixel separately). This process with this setup is not very time consuming, imaging samples is made a lot easier, and new research to further develop efficient light couplers are greatly benefitting from this setup. This as well as characterization of the waveguide peaks is going to be the study of the PhD student that is now working with the setup.

7. Suggestions

After the diode banks are repaired the setup should be working as it was when the author measured the experiments described in this thesis. Below are suggestions for further research written in short bullet points.

- More measurements can be made to fine tune the alignment of mirrors and lenses. This will increase the temporal resolution, as the setup in 2012 had a higher resolution.

- A solution to determine the temporal accuracy would be to execute multiple measurements of the same sample. As the position of the peaks have to be the same for every measurement, a standard deviation can be calculated.

- Measure the spectrum of the different pulses for example: pulsed output Tsunami, probe/gate beam, probe beam after interaction with sample and the Sum frequency generated signal.

- Image contrast can be increased by taking a "dark picture". This can be done before or after an image is taken. The dark image has to have the same integration time as the image, but the signal beam should be blocked. After this a software program like ImageJ can subtract the dark picture from the signal image. This will increase contrast drastically. This procedure is to take out the noise the camera makes itself.

- To also increase the quality of the images in the vertical plane, the decrease in quality is introduced due to lattice orientation in the gating crystal. A two image setup is proposed, when the first picture is made the crystal is at 0 degrees' position. For the second image the crystal has to be turned 90 degrees (and turn the polarizations as well of the gate and probe beam). After these two images have been taken, they are subtracted from each other in a software of choice. Also a beam splitter in the path of the signal beam has been taken into consideration, but to divert these to two different crystals is not recommended, as the intensity of the pulse will be decreased by half and the efficiency in up converting is quite low, the output would be too low to take an image.

- Measure the difference in cross convolution from the BBO and BiBO crystal, this will give an indication as to whether one of the two crystals has a longer decay time.
- Measure different kind of waveguide assemblies (without resonator, without resonator and bend) to determine the different peaks. This will be the study subject of the PhD student that is currently working with the setup.

- An addition to above stated recommendations is that the condition in the lab are far from stable, the temperature (especially after one o'clock) changes drastically, and the humidity is not sufficiently controlled. There is no dust filter in the lab itself, the density of dust is not at a minimum.

8. Bibliography

1. Weiner, A. *Ultrafast Optics (Wiley Series in Pure and Applied Optics)*. (2009).
2. Pattelli, L., Savo, R., Burresi, M. & Wiersma, D. S. Spatio-temporal visualization of light transport in complex photonic structures. **5,** 1–20 (2015).
3. Columbus, F. H. *developments in quantum physics*.
4. Pedrotti, F. *Introduction to optics (third edition)*. *Optics & Laser Technology* **21,** (2007).
5. Kasap, S. O. *Optoelectronics & Photonics: Principles & Practices (3nd Edition)*.
6. Sutherland, R. L., Mclean, D. G. & Kirkpatrick, S. *Handbook of Nonlinear Optics with contributions by*. *New York*
7. Ascroft, N. W. *Solid state physics*. (1976).
8. Francois, A., Riesen, N., Ji, H., Afshar V., S. & Monro, T. M. Polymer based whispering gallery mode laser for biosensing applications. *Appl. Phys. Lett.* **106,** 16–20 (2015).
9. Boyd, R. W. *Nonlinear Optics, 3th edition*. **3,** (2007).
10. Choy, M. M. & Byer, R. L. Accurate second-order susceptibility measurements of visable and ifrared nonlinear crystals. *Phys. Rev. B* **14,** 1693 – 1706 ST – Accurate second–order susceptibi (1976).
11. Spectra Physics. *Optical Parametric Oscillator (OPAL) Manual*. (2001).
12. Cortese, L. *Light transport in complex photonic structures : Scattering optimisation in white beetles*. (2015).
13. Ghotbi, M. & Ebrahim-Zadeh, M. Optical second harmonic generation properties of BiB3O6. *Opt. Express* **12,** 6002–6019 (2004).
14. Barthelemy, P. Anomalous Transport of Light. (2009).
15. Contini, D. *et al.* Photon migration through a turbid slab described by a model based on diffusion approximation. I. Theory. *Appl. Opt.* **36,** 4587–99 (1997).
16. Gersen, H. *et al.* Propagation of a femtosecond pulse in a microresonator visualized in time. *Opt. Lett.* **29,** 1291–1293 (2004).
17. Spectra-Physics. Tsunami Mode-locked Ti:sapphire Laser. *Physics (College. Park. Md).* 238 (2002).
18. Pattelli, L., Savo, R., Burresi, M. & Wiersma, D. S. Supplementary information: Spatio-temporal visualization of light transport in complex photonic structures. 1–20 (2015). doi:10.1038/lsa.2016.90
19. Hudson. Lectures on Elemantary Statistics and Probability. in 30–37 (1963).
20. Thorlabs. ThorLabs translation stage information. Available at: https://www.thorlabs.com/newgrouppage9.cfm?objectgroup_id=3961. (Accessed: 6th January 2016)
21. Shah, J. Ultrafast luminescence spectroscopy using sum frequency generation. *Quantum Electron. IEEE J.* **24,** 276–288 (1988).
22. HHS. *Onnauwkeurigheidsanalyse – Samenvatting*. 3 (2014).
23. Pattelli, L. Ultrafast time- and space-resolved investigation of diffused light transmission through strongly heterogeneous media. (2014).
24. Ming Cai, Oskar Painter, and K. J. V. Observation of Critical Coupling in a Fiber Taper to a Silica-Microsphere Whispering-Gallery Mode System. *Dep. Appl. Phys.* **85,** 74–77 (2000).
25. NOAA. emwave. Available at: http://www.livescience.com/38169-electromagnetism.html. (Accessed: 2nd March 2016)
26. University of Waikato. reflectie. (2012). Available at: http://sciencelearn.org.nz/Contexts/Light-and-Sight/Science-Ideas-and-Concepts/Reflection-of-light. (Accessed: 15th March 2016)
27. Bob, D. Laguerre-gaussian. Available at: https://commons.wikimedia.org/w/index.php?curid=4008320. (Accessed: 28th April 2016)
28. MPI, S. of light. wgm. Available at: http://www.nanowerk.com/nanotechnology-news/newsid=37462.php. (Accessed: 5th May 2016)

Appendix A – spatial resolution improvement

To first find the spatial resolution of the images made with the BBO crystal, an image is made through the optics set used when the paper images were made. The image made is a ruler which is lighted with white light from the front of the ruler. From this image it is possible to find the correspondence from a pixel to length, as can be seen from figure A-1. The image has been corrected for a little spherical aberration, so that all the pixels on the image plane will correspond to the same distance.

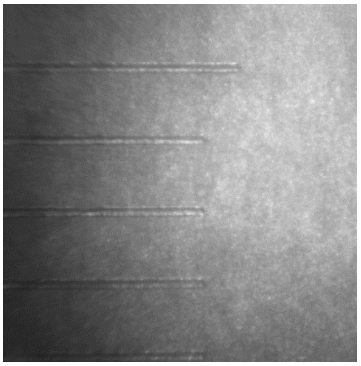

Figure A-1, the imaged ruler.

The distance between the stripes is measured three times on different location per stripe. The measurement point goes from the middle of the stripe to the next middle of the stripe. From this an average distance and standard deviation can be calculated.

The result for the BBO crystal used in the paper measurements is: 100±2 pix·mm^{-1}. The accuracy is calculated by the standard deviation on a population of 12 measurements.

To calculate the maximum spatial resolution of the paper measurement setup the up converted image of the target is used. In figure 2, there is a cropped version of the up converted image of the target, in which the author enhanced the contrast. The vertical alignment is very bad as previously stated, and it has been chosen that the last 3 lines (group 5, bottom left) is the maximum of the resolvement of the setup. This can be of course debated as it is still clear that they are three different lines. But the "smearing" of the line is so great that the lines are partially overlapping.

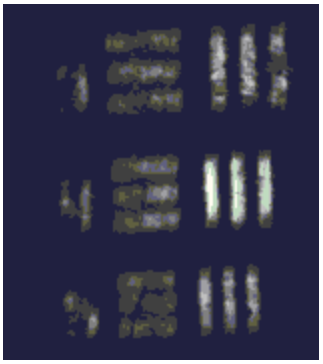

Figure A-2, the up converted target image.

The width of the lines is measured in the same way as the above measurements, which gives it an average width of 9±1 pix. To calculate the resolution, the following formula is used:

$$R_{\max} = \frac{9}{100} = 0,090 \text{ mm} \qquad \text{(A.1)}$$

In which R_{max} is the minimum object size that can still be imaged clearly.

The uncertainty is calculated by using the formula stated in the uncertainty analysis paper provided by The Hague University[22], this is the addition of the relative uncertainty:

$$\Delta R = \left(\frac{2}{100} + \frac{1}{9} \right) \cdot 0,09 = 0,01 \text{ mm} \qquad \text{(A.2)}$$

The result from the above analysis is that the maximum resolvement of the BBO crystal in this setup is: 90±10 μm. The uncertainty is quite high as the measurement of the pixels per millimeter is not of very high quality. This could be overcome by a more "high tech" method of measuring the distance-pixel ratio, using a Thorlabs Line per mm target.

As the crystal is switched from the BBO to BiBO, it is expected to have a better spatial accuracy. This is because of the difference in structure of both the crystals, and the decrease in thickness of the BiBO crystal (although the intensity will be less as there is less crystal volume where SFG can occur).

The BiBO crystal has a higher efficiency (a larger χ) so this decrease in intensity will not be linear to the thickness. This is a subject for more study.

As BiBO has a wider angle of acceptance for *k*-vectors, it is predicted that the spatial resolution will improve[18].

Now for the measurements made by the new crystal it is not necessary to make an image of a ruler as there is a known distance in the image itself (this is also not possible, as the laser is not working). The problem is that it is not known whether the light coming out of the output coupler is the smallest possible resolvement of the setup. But, it will give an indication if the spatial resolution has increased or decreased with the use of the new and thinner BiBO crystal.

The grating is 10 μm wide with a deviation of 0,2 (this deviation is the standard deviation the nanoscribe assembly has). The amount of pixels this corresponds to is 35 ± 2. This gives 3,5±0,2 $px \cdot \mu m^{-1}$ using the same method as described above.

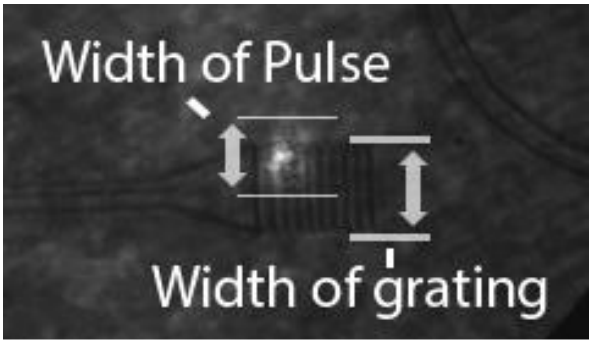

Figure A-3, the pulse coming out of the grating, with the grating image overlayed.

The width of the light pulse is something that is debatable. Here the author has chosen to be on the safe side, therefore a distance wider than the pulse is taken. The width is 28 pixels, which corresponds to 8±1 μm. This is a ten time increase of the spatial resolution, but as the above measurement, a few considerations should be taken into account. It is not known wheter the light that is coming out of the coupler is focused or divergent. It could actually be that the spatial resolution is even smaller, but at the moment it is not possible to measure this.

Appendix B – Whispering gallery mode resonators

A whispering gallery resonator is a ring in which a wave can travel on the outskirts of the ring by total internal reflection. First discovered in the st. Paul's church as somebody could stand with his face against the wall talking, and a listener could hear the voice only when he was in the path (close to the wall) of the sound wave. The wave bounces off the wall in very small increments, meaning the path between bouncing is small. A visual representation of this is given in figure B-1.

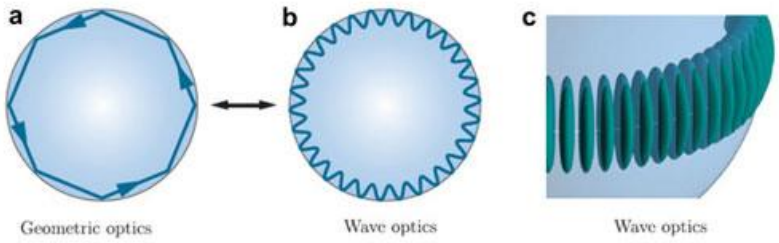

Figure B-1, three different views of light travelling inside a resonator (adapted from[28])

Light can exhibit the same pattern of travelling in this resonator, as long as the ring has a higher refractive index as its surroundings. As the light travels through the resonator it travels a distance of 2πr for one roundtrip (r being the radius of the circle). This leads to a time difference per round trip of:

$$\Delta t_m = \frac{2\pi r}{c} m \tag{B.1}$$

In which *m* is an integer and states the number of roundtrips the wave has done.

As the WGM resonator in this thesis is fed by a waveguide, and the introduction of light inside the resonator is done by evanescent wave coupling, the following expression gives an estimation of the ratio of intensity coupled into the WGMR with respect to the intensity inside the waveguide close to it[24]:

$$T = 1 - \frac{C}{1 + f \sin^2\left(\pi \frac{\nu}{\Delta\nu_{fsr}}\right)} \tag{B.2}$$

In which:

$\Delta\nu_{fsr}$	=	free spectral range	[m^{-1}]
f	=	finesse factor	[-]
C	=	resonator coupling coefficient	[-]
T	=	transmission ratio	[-]

Free spectral range stands for the distances in between modes, or it can be said that it is the spread of modes allowed in the resonator. C is the resonator coupling coefficient, meaning that for C is equal to one, no light will go through in the waveguide and all will be transferred to the resonator.

This can be calculated by:

$$C = 1 - \left(\frac{t - \gamma}{1 - \gamma t} \right)^2 \tag{B.3}$$

In which:

γ = resonator round trip factor [-]

The resonator round trip factor is an approximation of the ratio of how many light rays actually can make a round trip. The value is a number between 0 and 1, with one meaning that there are no losses (all light rays make a round trip) and 0 means that no ray can make a roundtrip (complete loss). And finally *f* is calculated by:

$$f = \frac{4\gamma t}{(1 - \gamma t)^2} \tag{B.4}$$

f stands for the losses inside the ring. As the ring is not a perfect mirror inside some losses will be present. Its relation to the *Q* factor is given by:

$$Q = \omega \tau_p \tag{B.5}$$

In which:

Q = quality factor [-]

T_p = photon decay time [s^{-1}]

The photon decay time is measured by switching off the feeding laser beam in a fast way (AOM preferably). When the switch-off time of the laser is known the difference between the switch off time and the measured output from the resonator gives the photon decay time. This is the time that the photon is still circulating the resonator. The longer the photon stays in the resonator, the higher the *Q*-factor is. The resonator that is being used in the measurements has a *Q* factor of around 800. This gives it 4,13 ps in the resonator after a pulse passes. This corresponds to 6,4 = 6 roundtrips.

As this concludes this appendix a side note is given: The resonator used in this thesis is one placed half on top of the waveguide, and therefore the calculation of transmission is far more intricate. Expression B.4 is merely an approximation specifically for a waveguide-resonator boundary in the same plane. Still the approximation gives an idea about the losses involved working with a whispering gallery mode resonator.

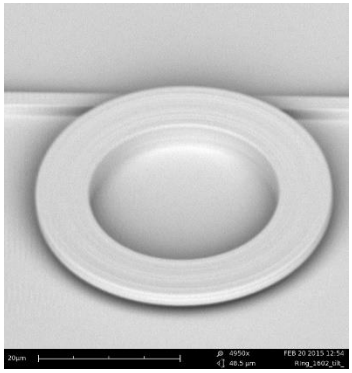

figure B-2, a SEM image of the resonator used in the experiments.

Appendix C – Temporal space in-between pulses

As the accuracy of the measurements are known, a more important matter can be discussed, the temporal resolution, or the amount of time the gate is "open" for the light to pass through. The cross convolution of the two pulses give a full width half maximum of 230 femtoseconds. As this is the only indication of the applied gating technique that can be measured it will be assumed that this is the maximum resolution possible with the current setup. Also the time between pulses is long enough so two different pulses will not interfere, as visually explained by figure C-1.

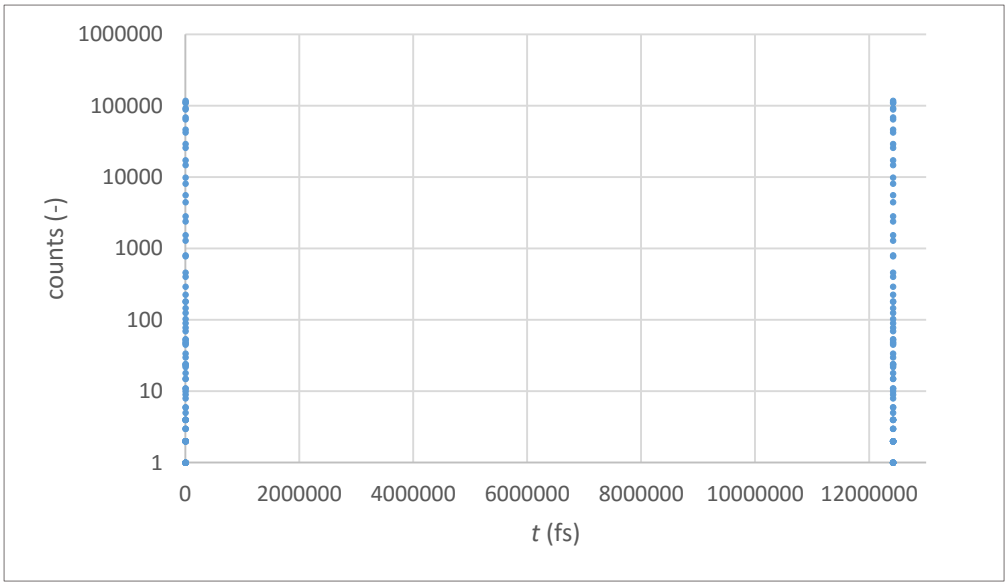

Figure C-1, a representation of the time between two pulses

The above graph is not a measurement as the translation stage is not long enough: The length needed to measure this is 3,75 meter. This graph is made by calculating the distance between the two pulses using the repetition rate of the pulsed laser and is only useable as a graphic explanation.

As the paper measurement pointed out the distance between two pulses is enough (the intensity of the delayed light output from the paper is zero at around 20 picoseconds). The time between the pulses is enough to measure the transport in paper without interference of a second pulse.

Appendix D – Calculating transport mean free path

The program that is used to calculate the transport mean free path is shown below, a quick overview:

First a matrix is indexed and the first column the values are inputted, the second the uncertainties and the last one is used as a changing value during every loop.

After this other variable are computed or accolated to the memory. The initial answer is first calculated by the vpasolve, this solving mechanism is explained in paragraph 4.4. The rest of the program is used to calculate the maximum error possible by using three for loops to check every answer that is possible. This is 3^3 times of calculation. All the different possibilities are saved in a three dimensional matrix, where later the maximum is found. This maximum gets subtracted from the initial value, the remaining number is the uncertainty given to the answer.

The output from the program using the variables already named in paragraph 5.2.1 is:

calculated value is 19.5 ± 4.8 um
with tau of: 1994 ± 9 fs
L of: 102.0 ± 2.000000 um
n of: 1.4 ± 0.05

The program is found on the next page.

```
Clc
clear all
% dex is the matrix where all the different outcomes are saved
dex=zeros(3,3,3);
debug=false;
% create matrix with values
%       val                             +-                              0
var=[(1/5.01571E-4)*1E-15,((1/5.01571E-4)-(1/5.0378E-04))*1E-15,  0; ...
   102E-6                          ,2E-6                           ,  0; ...
   1.4                             ,0.05                           ,  0   ];
% % additional variables
n=var(3,1);
A=504.332889-2641.00214*n+5923.699064*n^2-7376.355814*n^3+5507.53041*n^4-2463.357945*n^5+610.956547*n^6-64.8047*n^7;
syms B;
```

```
% % calculating initial answer
UP=(var(2,1)+(4/3)*A*B)^2;
BO=((1/3)*B*(3E8/var(3,1))*pi^2);
eqn=(var(1,1)==(UP/BO));
answer1=vpasolve(eqn,B);
outcome=answer1(1,1)/1E-6;

if debug==true
   fprintf('answer is: %f fs\n',outcome(1,1))
end

%       resetting variables.
var(:,3)=var(:,1);

for i=1:3;
   if i==1
      var(1,3)=var(1,1)+var(1,2);
      if debug==true;
         fprintf('i=1 %f fs\n',var(1,3)*1E15)
      end
   end
   if i==2
      var(1,3)=var(1,1)-var(1,2);
      if debug==true;
         fprintf('i=2 %f fs\n',var(1,3)*1E15)
      end
   end
   if i==3
      var(1,3)=var(1,1);
      if debug==true;
         fprintf('i=3 %f fs\n',var(1,3)*1E15)
      end
   end

   for j=1:3;
      if j==1
         var(2,3)=var(2,1)+var(2,2);
         if debug==true;
            fprintf('j=1 %f um \n',var(2,3)*1E6)
         end
      end
      if j==2
         var(2,3)=var(2,1)-var(2,2);
         if debug==true;
            fprintf('j=2 %f um\n',var(2,3)*1E6)
         end
      end
      if j==3
         var(2,3)=var(2,1);
         if debug==true;
            fprintf('j=3 %f um\n',var(2,3)*1E6)
         end
      end

      for k=1:3;
         if k==1
            var(3,3)=(var(3,1)+var(3,2));
            if debug==true;
               fprintf('k=1 %f \n',var(3,3))
            end
         end
         if k==2
            var(3,3)=var(3,1)-var(3,2);
            if debug==true;
               fprintf('k=2 %f \n',var(3,3))
            end

         end
         if k==3
            var(3,3)=var(3,1);
            if debug==true;
               fprintf('k=3 %f \n',var(3,3))
            end
         end

         % % setting up the equation
         UP=(var(2,3)+(4/3)*A*B)^2;
         BO=((1/3)*B*(3E8/var(3,3))*pi^2);
         eqn=(var(1,3)==(UP/BO));
         % % solving
         answer=vpasolve(eqn,B,outcome);
         % % indexing
         answer1=answer/1E-6;
         dex(i,j,k)=abs(outcome-answer1(1,1));

      end %k
   end %j
end %i

if debug==true;
   fprintf('uncertainties are:\n')
   disp(dex)
end

% taking average of all uncertain outcomes
unc=max(max(max(dex)));

fprintf('calculated value is %1.1f ± %1.1f um\n\n',outcome,unc);
fprintf('with tau of: %4.0f ± %2.0f
fs\n',var(1,1)*1E15,var(1,2)*1E15);
fprintf('       L of: %2.1f ± %f um\n',var(2,1)*1E6,var(2,2)*1E6);
fprintf('       n of: %1.1f  ± %1.2f\n',var(3,1),var(3,2));
```